

c. 2

INTERRELATIONSHIPS BETWEEN THERMAL HISTORY AND MECHANICAL PROPERTIES OF A SECONDARY HARDENING STEEL

Nareshchandra J. Kar  
(M. S. thesis)

December 1976

RECEIVED  
LAWRENCE  
BERKELEY LABORATORY

FEB 9 1977

LIBRARY AND  
DOCUMENTS SECTION

Prepared for the U. S. Energy Research and Development Administration under Contract W-7405-ENG-48

TWO-WEEK LOAN COPY

This is a Library Circulating Copy which may be borrowed for two weeks. For a personal retention copy, call Tech. Info. Division, Ext. 5716

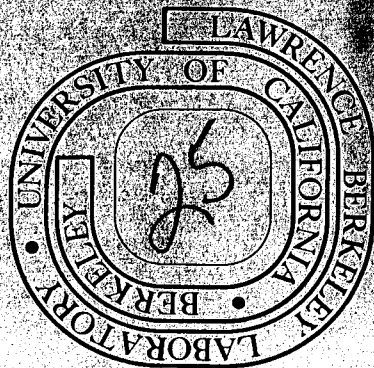


Table of Contents

ABSTRACT . . . . .	v
I. INTRODUCTION . . . . .	1
II. EXPERIMENTAL PROCEDURE . . . . .	3
A. Material Preparation . . . . .	3
B. Dilatometry . . . . .	3
C. Heat Treatments . . . . .	3
D. Mechanical Testing . . . . .	4
1. Tensile Testing . . . . .	4
2. Fracture Toughness Testing . . . . .	4
3. Hardness Testing . . . . .	5
E. X-Ray Measurements . . . . .	5
F. Optical Metallography . . . . .	5
G. Fractography . . . . .	6
H. Energy Dispersive Analysis of X-Rays . . . . .	6
III. RESULTS AND DISCUSSION . . . . .	7
A. Selection of Austenitization Treatment and Time- Temperature Paths . . . . .	7
B. Mechanical Properties . . . . .	8
C. Fractographic Analysis . . . . .	11
D. Two Step Austenitization Treatments . . . . .	13
E. Mechanical Properties with Heat Treatment Schedule 2A . . . . .	14
F. Fractography . . . . .	16
G. Mechanical Properties with Heat Treatment Schedule 2B . . . . .	17
H. Analysis of Alloy Carbides . . . . .	19

IV. CONCLUSIONS . . . . .	22
APPENDIX . . . . .	25
REFERENCES . . . . .	27
ACKNOWLEDGEMENTS . . . . .	29
TABLES . . . . .	30
FIGURE CAPTIONS . . . . .	36
FIGURES . . . . .	41

INTERRELATIONSHIPS BETWEEN THERMAL HISTORY AND  
MECHANICAL PROPERTIES OF A SECONDARY HARDENING STEEL

Nareshchandra J. Kar

Materials and Molecular Research Division, Lawrence Berkeley Laboratory  
and Department of Materials Science and Engineering,  
University of California, Berkeley, California 94720

ABSTRACT

Commercial secondary hardening steel, VASCO MA, has been subjected to modified heat treatments to introduce mixed microstructures of martensite and lower bainite. Dilatometry, tensile testing, hardness measurements and slow-bend testing have been carried out and the mechanical properties obtained have been correlated to microstructure using scanning electron microscopy and metallography. Duplex microstructures containing small amounts of lower bainite are found to show an increased toughness (at similar strength levels) on tempering in the secondary hardening range, as compared to initially fully martensitic microstructures. As the percentage of lower bainite in the duplex microstructures is increased, the secondary hardening peak is found to attenuate. The effect of different austenitization treatments on the secondary hardening behaviour, has also been studied. Thermal cycling (for grain refinement) at lower austenitization temperatures is found to reprecipitate out carbon, which has been taken into solution in earlier high temperature austenitization, thereby leading to a significant depletion in the strength of this secondary hardening steel. Alloy carbides, in the secondary hardening stage, have also been analyzed using energy dispersive analysis of X-rays.

## I. INTRODUCTION

The normal route to high strength in steels, has been by quenching, to form martensite or bainite, followed by tempering to eliminate brittleness, while still maintaining a high strength.<sup>1</sup> The three stages of tempering for plain-carbon steels, have been topics well explored by a number of investigators.<sup>2,3</sup> In plain-carbon steels, modification of martensite occurs by the gradual precipitation of iron carbide, i.e. initially  $\epsilon$  carbide and then cementite. The situation is radically altered when stronger carbide-forming elements are present. Chromium, vanadium, tungsten, molybdenum form carbides which are thermodynamically more stable than cementite. Consequently, if the tempering temperature is raised sufficiently, adequate opportunities are present for the diffusion of these elements to occur; a fine dispersion of alloy carbides is formed, which offsets the softening due to coarse cementite, thereby leading to an important strengthening mechanism in these alloy steels - secondary hardening.

Vasco MA is a commercial steel, which has established itself as a secondary hardening steel. However, the strength levels and attendant hardness of this high alloy steel are restricted, because as the strength and hardness of such quenched and tempered martensitic steels is increased, the ductility decreases.

In the quest for obtaining high strengths in modern-day steels, without sacrificing ductility, research workers have explored the bainitic route. Investigators have found that in high C steels, a

lower bainitic morphology is found to give significantly higher fracture toughness values (at similar strength levels), as compared to tempered twinned-martensitic structures.<sup>4,5</sup> Other research workers have also indicated that in bainitic steels, the secondary hardening peak is slightly retarded, as compared to martensitic steels.<sup>6</sup> Early work in 4340<sup>8</sup> has shown, that small amounts of bainite formed close to  $M_s$  temperature, coupled with a high temperature tempering treatment, improves hardenability, without deteriorating strength or ductility.

It was decided to explore the realm of mixed microstructures (martensite + lower bainite), so as to study the response of such microstructures to secondary hardening, with a view to enhance fracture properties, at attendant high strength levels. With advances in the field of fracture mechanics, it is now possible to measure parameters like plane-strain fracture toughness ( $K_{Ic}$ ) using slow-bend tests, and this, together with tensile testing, gives one a good handle on the mechanical properties of complex alloy steels.

Specific heat-treatments have been designed (with the aid of dilatometry) to obtain varying amounts of lower bainite + martensite, so that the response of mixed microstructures to secondary hardening can be studied, as also an insight into the various strength-toughness combinations can be obtained.

## II. EXPERIMENTAL PROCEDURE

### A. Material Preparation

The steel was received from Contour Sawblade Co., in the form of billets, 1 in. in diameter. These were homogenized in a vacuum furnace for 48 hrs. and then furnace-cooled. A chemical analysis was carried out from three different sections, and the typical alloy composition is shown in Table I.

### B. Dilatometry

Standard dilatometric specimens, were used on the Theta dilatometer shown in Fig. 1. The  $M_s$  temperature was found to be 220°C, and by carrying out isothermal temperature runs at intervals of 20°C, the time-temperature transformation (TTT) diagram in the region of interest, was determined. This is shown in Fig. 2.

### C. Heat Treatments

The initial set of austenitizing treatments were carried out in two resistance-heating furnaces, placed side-by side, using an argon atmosphere. Specimens were enclosed in stainless steel bags, filled with argon gas; these bags were pierced, prior to quenching in the isothermal bath. Isothermal treatments were carried out in saltpots, located beneath the furnaces. The salt was mechanically agitated to ensure a constant temperature throughout the saltpot. Specimens were finally quenched to room temperature using agitated quenching oil.

In the later set of heat-treatments, vertical tube furnaces with an argon atmosphere, were used for initial austenitization treatment. Second-step reaustenitization was carried out by up quenching into a saltpot containing high-temperature salt. Specimens were held at this temperature for specific times, then quenched to room temperature. The experimental set up is shown in Fig. 3. Subsequent tempering was also carried out in saltpots containing high-temperature salt.

Specimens used in all the heat treatments, were oversized tensile and three-point bend blanks. After heat-treatment, these were machined to final dimensions, using flood-cooling.

#### D. Mechanical Testing

##### 1. Tensile Testing

Tensile properties were determined using the 1 in. gage length,  $\frac{1}{4}$  in. diameter round specimen, shown in Fig. 4. Oversized specimens were heat treated and then ground to final dimensions, using flood cooling. Tests were conducted at room temperature using a 300 Kip MTS testing machine, at a cross-head speed of 0.04 in./min.

##### 2. Fracture Toughness Testing

Fracture toughness testing was carried out using three-point bend specimens, shown in Fig. 5. Tests were carried out on the 300 Kip MTS testing machine, with a modified set-up, visually displayed in Fig. 6. A crack-opening displacement (C.O.D.) gage was used to monitor the crack length. The three-point bend test specimens could not be precracked, and further details of how a reasonable plane-strain fracture toughness value,  $K_{Ic}$ , can be obtained from rounded notch three point

bend specimens is given in Appendix A.

### 3. Hardness Testing

Hardness values on the Rockwell C scale were obtained, using the Wilson Rockwell Hardness tester. Specimens were cut from broken bend specimens, mounted and polished by suitable metallographic techniques; an average of 10 readings per specimen, was taken.

#### E. X-Ray Measurements

Quantitative measurements of retained austenite were made using the Miller method; a Picker X-ray diffractometer, with a fixed horizontal stage, and  $\text{Cu K}_\alpha$  radiation was used. The scan angle covered was from  $40^\circ$  to  $100^\circ$ , to include the  $(111)_\gamma$ ,  $(311)_\gamma$ ,  $(220)_\gamma$ , and  $(222)_\gamma$  reflections. Specimens used were cut from fractured three-point bend specimens, polished and etched in a solution of 100 ml.  $\text{H}_2\text{O}_2$  + 4 ml. HF, to obtain a shiny surface. Each sample was run twice, rotating through  $90^\circ$  for the second run to minimize the effects of any preferred orientation that might exist.

A careful study by X-ray measurements, revealed that the amount of retained austenite, after a two hour tempering treatment, was too small to be identified by diffractometer measurements, i.e. less than 3-4%.

#### F. Optical Metallography

Specimens for optical metallography were cut from broken three point bend specimens. These were mounted in Koldmount, abraded on silicon carbide papers down to 600 grit, polished on a  $6\mu$  and then  $1\mu$  diamond wheel. Final polishing was done in a syntron, using  $0.05\mu$

Al<sub>2</sub>O<sub>3</sub> solution. In order to reveal prior austenitic grain boundaries and undissolved carbides, etching was carried out using an etchant that consisted of 5 gm. picric acid in 100 cc water saturated with dodecylbenzene sulfonate. Martensite/bainite microstructure was revealed using a 5% nital etch.

#### G. Fractography

Fracture surfaces of the three point bend specimens were examined using a AMR scanning electron microscope, at an operating voltage of 20 kV. During preparation for observation, the fracture surfaces were protected with acetate tape. The acetate tape was later stripped off and the specimens were cleaned in acetone.

#### H. Energy Dispersive Analysis of X-Rays

Energy Dispersive Analysis of X-Rays (EDAX) techniques were used to analyze the matrix and carbides present in the various specimens. Broken three point bend specimens were cut and mounted in Koldmount and polished similar to optical metallography specimens. A picral etch was used to reveal prior austenite grain boundaries and alloy carbides. The EDAX stage on the AMR scanning electron microscope was used and the analysis was facilitated by the use of pre-programmed cassettes on a mini-computer appended to the AMR scanning electron microscope.

When carrying out the analysis, sufficiently large precipitate particles were selected, and the aperture of the beam was narrowed so as to eliminate errors that might arise from the matrix.

### III. RESULTS AND DISCUSSION

#### A. Selection of Austenitization Treatment and Time-Temperature Paths

Commercial austenitization of Vasco MA secondary hardening steel involves preheating at 900°C (30 mins.), austenitization at 1100°C and an oil quench. Although this solution treatment yields a structure that is almost completely martensitic, a significant number of carbides are found, which do not dissolve during the solution treatment. A typical example is shown in Fig. 7. As has been well established, the presence of undissolved carbides is deleterious to fracture toughness.<sup>9</sup> Hence, a systematic schedule of test treatments were carried out, using austenitization temperatures periodically increasing from 1100°C to 1350°C, and times varying from 20 minutes to 2 hours. These higher temperatures do not completely eliminate the undissolved carbide distribution, but promote a large amount of grain-growth. Hence, this trend of reducing undissolved carbide fraction, by using higher solution treatment temperatures was not pursued.

The commercial austenitization schedule was slightly modified to include an isothermal path. Isothermal times and temperatures were determined with the aid of the TTT diagram, which was determined on the Theta dilatometer. Paths were so designed so as to have varying percentages of lower bainite and martensite.

A schematic diagram showing the heat treatment schedule is presented in Fig. 8. The steel was preheated at 900°C for 30 mins., then austenitized at 1100°C for 15 mins. A rapid quench was carried out to isothermal transformation temperature (250°C/210°C) and specimens were held at this temperature for periods ranging from 60 mins. to 180 min. followed by an oil quench to room temperature. Tempering was carried out at 550°C for a period of 2 hours.

#### B. Mechanical Properties

Isothermal treatments at 210°C (a little below  $M_s$ ) produce a mixed morphology of martensite + lower bainite. The hardness versus tempering temperature curve of the duplex microstructure (after 1 hour isothermal time) is shown in Fig. 9. This duplex structure is found to show a secondary hardening peak at 550°C, analogous to a fully martensitic microstructure. Retained austenite measurements using the X-ray diffractometer indicate that a 2 hr. tempering treatment is sufficient to transform any retained austenite, that may be present. From Fig. 9 it is evident that double and triple tempers do not increase hardness levels significantly, and hence, 2 hr. tempering times were pursued in all the treatments.

Tensile test and fracture toughness results are presented in Table II. The duplex structure obtained after a 1 hr. isothermal treatment is found to have yield and ultimate tensile strengths close to a fully martensitic microstructure. The calculated plane strain fracture toughness (as measured by three point bend tests), however,

is found to increase from  $84 \text{ ksi-in}^{1/2}$  for a fully martensitic microstructure, to  $93 \text{ ksi-in}^{1/2}$  for a duplex structure.

Although no direct evidence of a twinned martensite was obtained, it would not be out of bounds to speculate that this high C, high alloy steel, would essentially be twinned martensitic, if subjected to an uninterrupted quench. Thomas et al.<sup>4,5</sup> have shown that a wide range of alloys exhibit reduced fracture toughness values for twinned martensitic microstructures as compared to lower bainitic structures. Thus, a duplex microstructure (containing small amounts of lower bainite) is likely to show an increase in fracture toughness, as compared to a fully martensitic microstructure, because of a reduction in the volume fraction of twinned martensite formed. Other recent investigations have also found duplex microstructures exhibiting very high fracture toughness values.<sup>7</sup> It may also be suggested that the isothermal transformation carried out, helps to reduce the transformation strain associated with the formation of martensite, thereby reducing the tendency towards quench cracking.

On increasing the  $210^\circ\text{C}$  isothermal transformation time, the yield and ultimate tensile strengths of the duplex structure are found to decrease; this is visually shown in Fig. 10. From Table II, it is seen that as the percentage of lower bainite formed increases, the attainable strength levels are found to decrease, although the calculated  $K_{Ic}$  values do not show a drastic change. The hardness profiles (Fig. 11) are analogous to the strength levels, dropping from  $R_c 60$  to  $R_c 58$ , as the isothermal transformation time is increased from 60 mins. to 180 mins.

Thus, the results seem to indicate that as the volume fraction of lower bainite in the duplex microstructures is increased (by increasing isothermal times), the attainable strength levels (on tempering in the secondary hardening range) and consequently, the hardness levels, are found to decrease. Hence, an increasing percentage of lower bainite, is likely to attenuate the secondary hardening response in a duplex microstructure.

250°C isothermal transformations: Isothermal transformations above  $M_s$ , are found to produce duplex structures of martensite and bainite, whose properties are shown in Table III and schematically shown in Fig. 12. As the tempering temperature is increased, the yield and ultimate tensile strengths peak at a temperature of 550°C, analogous to the hardness vs. tempering curves of Fig. 13. These duplex structures exhibit significantly high strength levels (on tempering in the secondary hardening range); however, fracture toughness measurements by three-point bend testing show that the fracture toughness of these higher temperature isothermal transformation products has dropped drastically to a low value of 23 ksi-in<sup>1/2</sup>, as shown in Fig. 14. Thomas et al.,<sup>4</sup> report similar results in their steels. They show that with increasing isothermal transformation temperatures, there is a coarsening of carbide particles, which lowers toughness. Although the TTT diagram plotted did not indicate two separate C curves, it is felt that the 250°C isothermal transformation may have introduced some upper bainite into the duplex structure. Upper bainite is known to exhibit very poor fracture toughness, because of the presence of interlath

carbides that cause embrittlement.<sup>10</sup> This may well account for the very poor toughness in the 250°C treatments.

Figure 12 compares the yield and ultimate tensile strengths obtained in the 250°C/210°C isothermal treatments, at different tempering temperatures. Duplex structures obtained by the 210°C isothermal treatment show significantly higher yield and ultimate tensile strengths, as compared to the 250°C treatments. This may be explained as follows. On quenching to 210°C (i.e. below  $M_s$ ), from the solution treatment temperature, the first transformation product to form from the austenite is high C martensite; this probably accounts for the increased yield strengths of the 210°C treatments, as compared to the higher temperature isothermal treatments, where the first transformation products to form from the austenite decomposition are likely to be upper and/or lower bainite. Hence, the yield and ultimate tensile strengths for the 210°C isothermals lie above the corresponding values for the 250°C treatments. As mentioned earlier, the curves in Fig. 12 show peaks on tempering at 550°C, similar to the hardness/tempering temperature curves; thus, the secondary hardening response of a mixed microstructure, is essentially unaltered with respect to temperature range, although higher isothermal transformation temperatures tend to lower hardness and strength. This is visually depicted in Fig. 11.

### C. Fractographic Analysis

Figures 15-16 illustrate the fracture morphology of the three point bend test specimens, tested at room temperature. Figure 15a, clearly illustrates that a 210°C isothermal (2 hrs.) produces a fracture

mode that is primarily dimpled rupture (microvoid coalescence). An enlarged view of this fracture surface is presented in Fig. 15b. As is evident from the fractographs, the high value of fracture toughness ( $K_{Ic}$  calculated) associated with this treatment may be accounted for by the large amount of dimpled rupture present during the failure of this specimen. As shown in Fig. 16a with increasing isothermal transformation time, the transgranular mode of fracture appears to be essentially quasi-cleavage.

The fracture surfaces of isothermal treatments above  $M_s$ , are shown in Figs. 17-19. The transgranular mode of fracture essentially exhibits quasi-cleavage facets. Figure 17b, shows an appreciable volume fraction of coarse, brittle carbides that are present in the matrix. Fig. 18a, and b, shows the same 250°C duplex structure after tempering at 400°C. The microstructures, from different regions demonstrate that coarse carbide particles are present all throughout the matrix. This particular treatment shows a very low calculated  $K_{Ic}$  value, i.e. 4.23 ksi-in<sup>1/2</sup>. This is likely to be attributed to crack nucleation by tearing at the carbide-matrix interface. Figure 19a shows the fracture surface of the three-point bend specimen. The fracture surface appears to show quasi-cleavage features.

Thus, poor fracture toughness obtained after 250°C isothermal treatments is likely to be attributed to: 1) some presence of upper bainite, and 2) the presence of a coarse distribution of carbides, which may be interlath carbides reported in upper bainite.

Das et al.,<sup>4</sup> have investigated mixed microstructures in a series of Fe-Ni-Co-C steels. They report that on tempering, mixed

microstructures exhibit a greater increase in yield strength and fracture toughness, for greater amounts of martensite present. The present results on the secondary hardening steel, differ in the fracture toughness aspect. Das et al. also find that with increasing transformation temperatures, the strength and toughness are found to decrease. They associate these with coarse carbide precipitation at higher transformation temperatures. The present results are in agreement with these. With an increase in isothermal transformation temperatures, carbide particles are found to coarsen. Unless these precipitate particles can deform with the matrix, these coarse carbides will act as stress raisers and crack nucleators.<sup>11-12</sup> Similar observations in a 9Ni-4Co-0.4C steel have also been made by Pascover and Matas.<sup>13</sup>

On the basis of the data obtained, it may be suggested that optimum mechanical properties of a duplex microstructure are obtained at transformation temperatures slightly below  $M_s$ .

#### D. Two Step Austenitization Treatments

The solution treatment schedule shown in Fig. 8, is found to leave some undissolved carbides. A periodic series of tests, using high austenitization temperatures of upto 1350°C for a period of 2 hours would not completely eliminate the undissolved carbides; there was a dramatic increase in the grain size of the prior austenite grains.

The need for a fine-grained microstructure cannot be adequately stressed. A finer grain size implies a larger grain boundary area, providing for a smaller coverage of grain boundaries by the segregation

of embrittling constituents.<sup>14</sup> A finer grain size is also found to lower the ductile-brittle transition temperature.<sup>15-16</sup> It is known that the smaller the grain size, the greater is the energy absorbed during fracture and the more difficult is the process of crack propagation.<sup>17</sup>

Thus, a two-step austenitization treatment was planned. This involved the use of high solution treatment temperatures to take more C into solution, and a second austenitization at a lower temperature, to obtain a fine-grain microstructure. This is schematically presented in Fig. 20. Schedule 2A refers to quenched and tempered treatments, schedule 2B is for isothermal treatments.

The first austenitization step consisted of austenitizing at 1200°C. The solution treatment temperature was raised from the earlier 1100°C to take more C into solution. Specimens were then step-quenched to room temperature. In the second austenitization cycle, reheating in the vertical tube furnaces was found to be slow, giving sufficient time for coarse carbides to come out of solution. Hence, an instantaneous upquench was carried out. Specimens were upquenched to a temperature of 897°C using a saltpot containing high temperature salt.

#### E. Mechanical Properties with Heat Treatment Schedule 2A

The tensile properties of Vasco MA steel subjected to a cyclic treatment, Schedule 2A, are listed in Table IV and shown in Fig. 21. Three point bend testing has also been carried out, and as described in Appendix A, the fracture toughness parameter  $K_{Ic}$  has been calculated using the Heald model.<sup>18</sup> The hardness vs tempering temperature curve

is shown in Fig. 22. The hardness values are found to be relatively low, as compared to the same steel subjected to Schedule 1. As the tempering temperature is increased, hardness rises at 400°C, and there is essentially only a very slight change in hardness on tempering at 550°C. The unexpected drop in hardness from  $R_c 60$  (in Schedule 1), to  $R_c 47$  may lead one to suspect that C was lost during the heat treatment. A C analysis was carried out and the results indicate that no C was lost either during the first stage austenitization in the tube furnace, or during subsequent upquench in the saltpot.

This leads one to infer that carbides have reprecipitated out of austenite, during the second stage upquench. A pilot set of tests were carried out and even brief times of a 2 min. upquench, were found to produce a similar low hardness of  $R_c 45-47$ . Hence, the reprecipitation of carbides out of solution, has essentially altered the morphology and alloy composition of the steel, and the mechanical properties obtained should be different from those obtained by the previous schedule. Dilatometric measurements indicate that the two step cycle has raised the  $M_s$  by 15°C, to 235°C.

The tensile and fracture properties listed in Table IV and Fig. 21 indicate that the yield and ultimate tensile strengths peak at a tempering temperature of 400°C. Thus, one definite effect of thermal cycling has been to shift the secondary hardening peak from the earlier 550°C to 400°C, as well as to significantly attenuate the peak. A comparative analysis of the alloy carbides present at these two temperatures has been made and will be discussed.

From Fig. 21, it is found that the  $K_{Ic}$  vs. tempering temperature curve is found to show an extremum at 400°C. The peak value is much lower than that obtained by using Schedule 1. A 500°C temper is found to lower the  $K_{Ic}$  value, and this may be attributed to the coarsening of alloy carbides which act as stress raisers and do not deform with the matrix. The  $K_{Ic}$  curve in Fig. 21 also shows a large drop on tempering at 300°C. Speich et al.<sup>2,19</sup> have indicated that if tempering is carried out between 230°C and 370°C, embrittlement occurs in a number of different AISI steels. This phenomenon is termed "500°F embrittlement". In the present investigation, there is insufficient evidence to conclusively ascertain if the observed  $K_{Ic}$  decrease on a 300°C temper was due to a similar embrittlement.

#### F. Fractography

Fractography of the three point bend specimens was carried out and is presented in Figs. 23-25. On tempering at 400°C, a fine dispersion of alloy carbides is seen in the matrix (Fig. 24b) and the fracture surfaces show a mixed mode of fracture - partly intergranular and partly quasi-cleavage; different regions of the 400°C temper specimen are shown.

Figure 25a, shows the microstructure obtained on tempering at 550°C. Coarse carbides can distinctly be seen in the matrix. Figure 25b shows the fracture surfaces. The mode of fracture primarily exhibits quasi-cleavage; carbides can also be seen at d and e.

G. Mechanical Properties with Heat Treatment Schedule 2B

Isothermal transformations at two different temperatures have been carried out. The tensile and fracture toughness properties are shown in Table V and visually depicted in Figs. 26 & 27. From Fig. 26, it is seen that for the same tempering treatment (ie. 550°C) with increasing isothermal time, the yield and tensile strengths increase, although there is essentially no change in the calculated fracture toughness.

On raising the isothermal transformation temperature, (250°C), the yield and ultimate tensile strengths of the duplex structures are found to lie below the corresponding values in the 210°C treatments. Das et al.<sup>4</sup> have found similar results in a series of Fe-Ni-Co-C steels. Fracture toughness for the 250°C treatments is found to be slightly higher than for the 210°C treatments. One may speculate that the higher temperature isothermal tends to reduce the amount of twinned martensite, that is found to occur in such highly alloyed steels, and this may partly be responsible for the increased fracture toughness.

Figure 28 shows the microstructure obtained after the thermally cycled steel was subjected to an isothermal transformation at 250°C for a period of 30 hours, i.e. a fully bainitic structure. On tempering at 550°C for 2 hrs., this structure shows a yield strength of 148.2 ksi and the fracture toughness is found to be 52 ksi-in<sup>1/2</sup>. Hehemann et al.<sup>8</sup> working on the effect of bainite on 4340, suggest that in duplex microstructures formed close to  $M_s$ , if tempering is carried out at elevated temperatures, the yield strength becomes virtually independent of microstructure. The data obtained in the present investigation

(plotted in Fig. 30) seems to indicate that beyond a certain isothermal time, the yield strength remains the same, independent of the amount of bainite formed. Thus the results seem to be in agreement with the observations of Hehemann et al.<sup>8</sup>

Table VI compares the tensile properties and fracture toughness of a fully martensitic vs. a fully bainitic structure; both of these have been tempered at 550°C for a period of two hours. The martensitic structure shows a slightly higher yield strength, but there is essentially no change in the ultimate tensile strength and fracture toughness between the two initially different morphologies.

Figures 31-32 shows the fracture surfaces of the three point bend specimens. River patterns, characteristic of quasi-cleavage are seen in the fully bainitic structure.

The results seem to indicate that in the secondary hardening steel, on thermal cycling, coarse carbides precipitate out of solution. Thus, the steel is altered, having a lower C, lower alloy content. Isothermal transformations at two different temperatures, give duplex structures. Increasing percentages of bainite do not drastically alter the yield and ultimate tensile strengths, and the calculated fracture toughness, remains almost the same. The controlling factor contributing to the low  $K_{Ic}$  value of 52 ksi-in<sup>1/2</sup> as compared to the previously attained 90 ksi-in<sup>1/2</sup> (using Schedule 1), probably is the presence of reprecipitated carbides. These carbides could act as a strong barrier for the movement of dislocations and could induce high stress concentrations, leading to crack nucleation.<sup>5,12</sup>

Figures 33-34 depict the effect of thermal cycling on the tensile and fracture toughness properties of the Vasco MA secondary hardening steel. As has been mentioned, re-austenitization at 900°C (to refine the grain size) causes carbides to reprecipitate out of solution, thereby altering the morphology and alloy composition. As a consequence, there are precipitous drops in the tensile properties and fracture toughness, as have been shown by the results in Tables IV and V. The secondary hardening characteristics are also altered, and there is a steep drop in hardness on tempering, from the earlier  $R_c 60$  to  $R_c 45$ .

#### H. Analysis of Alloy Carbides

One of the most important aspects of a secondary hardening steel, is the precipitation of alloy carbides, on tempering at higher temperatures. The tempering of a secondary hardening steel can be divided into four stages. In the first three stages, modifications occur similar to plain carbon steels - initially  $\epsilon$  carbide precipitates, and at higher temperatures there is a precipitation of cementite. In secondary hardening steels, however, at higher tempering temperatures, a fine dispersion of alloy carbides are formed, which offset the softening due to coarse cementite, thereby leading to an appreciable increase in the hardness and strength of such steels.

It has been found that the replacement of cementite occurs in two ways: 1,21-22

i) By in situ transformation, where the cementite particles are gradually transformed to the alloy carbide, by inward diffusion of the alloying element;

ii) By separate nucleation of the alloy carbide during a period when the cementite particles go back into solution in the ferrite.

Earlier work has shown that  $\text{Mo}_2\text{C}$  is the effective carbide in molybdenum steels,<sup>24,25</sup> while  $\text{V}_4\text{C}_3$  is responsible for the strengthening observed in vanadium steels.<sup>20</sup> Baker and Nutting,<sup>26</sup> working on a 0.22 C, Cr-Mo-V-W steel, find that vanadium carbide is the principal carbide in the secondary hardening range, whilst a Mo-V steel shows  $\text{V}_4\text{C}_3 + \text{M}_6\text{C}$  carbides.

In the present investigation, an interesting aspect was to determine what alloy carbides existed in the 0.5C + 12% alloying elements steel, whose composition is shown in Table I. Complexities in the steel would not permit the making of suitable thin foils, and hence, electron microscopic examinations could not be suitably carried out.

It was decided to analyze the alloy carbides using Energy Dispersive Analysis of X-Rays (EDAX). The results are shown in Figs. 35-39.

Figure 35 shows the EDAX analysis of the alloy carbides that account for secondary hardening in an initially martensitic matrix, obtained by using Schedule 1. The percentages shown are weight percent, and from the data, it is evident that the alloy carbide was primarily a W+Mo carbide. The carbide being analyzed was sufficiently large (Fig. 7) to prevent counts from the matrix being taken.

Figures 36-37 show the EDAX analysis of alloy carbides after the steel was subjected to a thermal cycle, i.e. Schedule 2. As has been discussed, a reprecipitation of carbides in the second austenitizing

cycle has effectively altered the secondary hardening characteristics and the alloy composition. The EDAX analysis for specimen 303 (tempered at 400°C) indicates that a W+Mo carbide accounts for the increase in strength, at this temperature. On tempering at 550°C, the hardness level practically remains the same as at 400°C, but there is a drop in the  $K_{Ic}$  value. EDAX analysis of specimen 302 shows that the alloy carbide primarily responsible for strengthening is a molybdenum carbide. Previous work on secondary hardening steels report  $Mo_2C$  as one of the likely carbides to be present in the temperature range 500-600°C. Thus,  $Mo_2C$  is probably the attendant alloy carbide in specimen 302.

Figure 38 shows three adjacent carbides that have been analysed on the EDAX. Carbides a and c are primarily  $Mo_2C$ , whilst carbide b also shows traces of V in it. (Fig. 39)

One other important aspect of this analysis is that the EDAX analysis of the 550°C carbides, shows a high percentage of Mn present in the carbides of specimen 302, whereas the matrix has negligible amounts of Mn present. Though Mn is unlikely to form a carbide, it is likely that some MnS inclusions may be present, which together with coarse alloy carbides, may well be responsible for the observed drop in fracture toughness, on tempering at 550°C.

#### IV. CONCLUSIONS

Based on the results and discussion, the following conclusions have been made:

1. Dilatometric techniques have been used to determine the TTT diagram of the Vasco MA secondary hardening steel. This diagram has been used to design specific time-temperature isothermal paths, to give duplex microstructures of lower bainite and martensite.

2. Duplex microstructures exhibit a secondary hardening peak in the same temperature range as fully martensitic microstructures. The secondary hardening peak is attenuated, as the percentage of bainite increases. X-Ray measurements show that no retained austenite is present subsequent to a 2 hr. temper. EDAX analysis shows that a W+Mo carbide is responsible for high temperature strengthening.

3. Duplex microstructures containing small amounts of lower bainite show an increase in fracture toughness at similar strength levels, as compared to fully martensitic structures. This is attributed to the decrease in volume fraction of twinned martensite.

4. With increasing isothermal transformation temperatures, there is a decrease in strength levels and fracture toughness is found to drop sharply. This is reported to be due to increased carbide coarsening at higher isothermal temperatures, and/or the presence of some upper bainite.

5. Fracture surfaces of high strength-high toughness alloys primarily indicate a dimpled mode of fracture. Other treatments show

a transgranular mode of cleavage fracture, with quasi-cleavage facets.

6. Commercial austenitization schedules leave undissolved carbides in parent austenite. Higher austenitization temperatures do not completely eliminate undissolved carbides; a large increase in grain size occurs.

7. Thermal cycling using high solution temperatures and a second low temperature austenitization, is found to reprecipitate carbides; thus the alloy morphology and composition are altered. As a consequence, secondary hardening is considerably attenuated, and occurs in a lower temperature range.

8. Quenched and tempered structures after a thermal cycle exhibit lower strength-toughness combinations. EDAX analysis reveals that a W+Mo carbide is responsible for secondary hardening observed at 400°C. Tempering at 550°C promotes the formation of  $\text{Mo}_2\text{C}$ , with traces of vanadium carbide. A drop in fracture toughness at this temperature is associated with carbide coarsening and the presence of Mn inclusions.

9. Isothermal transformations (after thermal cycling) indicate that beyond a certain percentage of bainite, the yield strength of the duplex microstructures virtually becomes independent of the proportion of microconstituents.

10. Optimum strength-toughness combinations are obtained by carrying out isothermal transformations for short periods of time, at temperatures very close to  $M_s$ . The reduction in volume fraction of twinned martensite enhances toughness.

11. The Heald model for obtaining reasonable estimates of plane strain fracture toughness, from rounded notch three point bend testing has been successfully used.

APPENDIX

Fracture Toughness Testing

Fracture toughness testing was carried out using three point bend testing. The three point bend test specimens were designed as per ASTM specifications,<sup>28</sup> and a typical specimen is shown in Fig. 4. It was not possible to fatigue precrack these specimens as the crack growth in these brittle specimens was difficult to control and hence rounded notch specimens were used, with a 0.004 in. root radius. The MTS testing machine, with a modified set-up (Fig. 6) was used. Static Charpy tests are not very sensitive to small changes in fracture toughness in such high strength, brittle materials, and hence were not used.

The apparent fracture toughness is calculated from the load displacement curve obtained, as per ASTM specifications:

$$K_{app} = (P_q s / bw^{3/2}) \cdot f\left(\frac{a}{w}\right)$$

where

$$f\left(\frac{a}{w}\right) = 2.9\left(\frac{a}{w}\right)^{1/2} - 4.6\left(\frac{a}{w}\right)^{3/2} + 21.8\left(\frac{a}{w}\right)^{5/2} - 37.6\left(\frac{a}{w}\right)^{7/2} + 38.7\left(\frac{a}{w}\right)^{9/2}$$

$P_q$  = load

$s$  = span length

$b$  = thickness of specimen

$a$  = crack length

$w$  = depth of specimen.

A reasonable estimate of plane strain fracture toughness  $K_{Ic}$  is obtained from non-valid ASTM tests, using a model developed by Heald, Worthington and Spink.<sup>18</sup> This model can be applied to tests that are non-valid w.r.t. the notch being semi-elliptical or circular rather than a sharp crack.

$K_{app}$  is related to  $K_{Ic}$  by:

$$K_{app}(\rho) = \frac{(\pi c)^{1/2} \sigma_u}{\left[1 + \left(\frac{\rho}{c}\right)^{1/2}\right]} \left( \frac{2}{\pi} \sec^{-1} \left[ \exp \frac{(\pi K_{Ic}^2)}{8\sigma_u^2 c} \right] + \left(\frac{\rho}{c}\right)^{1/2} \right)$$

where  $\rho$  = root radius

$\sigma_u$  = ultimate tensile strength

$c$  = crack length

For three-point bend specimens, this reduces to

$$K_{Ic} = \left( \frac{8\sigma_u^2}{\pi} \cdot 0.19 \ln \sec \left[ \frac{1.145 K_{app} \frac{\pi}{2}}{(\pi)^{1/2} \cdot (0.19)^{1/2}} - \frac{\pi}{2} (0.145) \right] \right)^{1/2}$$

REFERENCES

1. R. W. Honeycombe, H. J. Harding, J. J. Irani, High Strength Materials, ed. V. F. Zackay (John Wiley & Sons, Inc., New York), 1965, p.213.
2. G. R. Speich and W. C. Leslie, Met. Trans. 3, 1043-1054 (1973).
3. W. C. Leslie, R. M. Fisher and N. Sen, Acta Met. 7, 632-644 (1959).
4. S. K. Das and G. Thomas, Trans. ASM 62, 659 (1969).
5. D. Huang and G. Thomas, Met. Trans. 2, 1587-1598 (1971).
6. F. B. Pickering, Precipitation Processes in Steels, ISI Spec. Report No. 64 (The Iron & Steel Institute, London) 1959, p.23-43.
7. B. V. N. Rao, M. S. Thesis, LBL-3794, University of California, Berkeley (1975).
8. R. F. Hehemann, V. J. Luhan, A. R. Troiano, ASM Trans. Quart. 46, 1557 (1954).
9. V. F. Zackay, E. R. Parker, R. D. Goolsby, W. E. Wood, Nat. Physical Science 236, 108 (1972).
10. G. Thomas, Iron & Steel International 46, 451 (1973).
11. E. R. Parker, V. F. Zackay, Fracture Mechanics 7, 371-375 (1975).
12. T. Tom, D-Eng. Thesis, LBL-1856, University of California, Berkeley (1973).
13. J. S. Pascover and S. J. Matas, ASTM STP 370, Am. Soc. Testing Mater. 30 (1965).
14. G. Clark, R. O. Ritchie, J. F. Knott, Nat. Physical Science 239, 104-106 (1972).

15. N. J. Petch, *Phil. Mag.* 3, 1089 (1958).
16. R. A. Grange, *Met. Trans.* 2, 65 (1971).
17. J. R. Low, Jr., Fracture, eds. B. L. Averbach et al, (MIT Press, Cambridge, Mass.) 68, 1959.
18. P. T. Heald, G. Spink and P. Worthington, *Mater. Sci. & Eng.* 10, 129 (1972).
19. R. L. Rickett and J. M. Hodge, *Proc. ASTM*, 931-944 (1951).
20. E. Tekin, P. M. Kelly, *JISI* 203, 715 (1965).
21. R. W. Honeycombe, Metallurgical Developments in High Alloy Steels, ISI Spec. Report No. 86 (The Iron & Steel Institute, London) 1-14 (1964).
22. K. Kuo, *JISI* 184, 258-268 (1956).
23. E. Smith and J. Nutting, *JISI* 187, 314-329 (1957).
24. R. Goolsby, Ph.D. Thesis, LBL-405, University of California, Berkeley (1971).
25. A. K. Seal and R. W. Honeycombe, *JISI* 188, 343-350 (1958).
26. R. G. Baker and J. Nutting, Precipitation Processes in Steel, ISI Spec. Report No. 64 (The Iron & Steel Institute, London) 1-22 (1959).
27. R. L. Miller, *Trans. of the ASM* 57, 892 (1964).
28. Annual of ASTM Standards, E399, American Society for Testing of Materials, Pa (1973).

#### ACKNOWLEDGEMENTS

The author wishes to express his gratitude to Professor Earl R. Parker and Professor Victor F. Zackay for their guidance and encouragement throughout this investigation. Appreciation is also extended to Professor Frank Hauser for his review of this manuscript and to Dr. R. O. Ritchie for helpful discussions on slow-bend testing.

The assistance of the support staff of the Molecular & Materials Research Division of the Lawrence Berkeley Laboratory is also acknowledged. In particular, the author wishes to recognize "Pat" Patenaude, Ed Edwards (machining) John Holthuis (alloy preparation), Sandra Stewart (purchasing), Don Krieger (mechanical testing), Lee Johnson (metallography), Alice Ramirez (manuscript preparation) and Evelyn Grant (line drawings).

I would also like to thank Tom Lechtenberg and my brother, Ramesh Kar, for valuable suggestions. Finally, I would like to thank my parents and the members of my family, who with their constant encouragement, have helped make study at Berkeley a thoroughly enjoyable one.

This research was supported by the U. S. Energy Research and Development Administration through the Materials and Molecular Research Division of the Lawrence Berkeley Laboratory.

Table I. Alloy Composition of Vasco 'MA'

C	Si	W	Cr	V	Mo	Mn	S	P
0.5	0.22	2	4.5	1	2.75	0.08	0.016	0.015

Table II. Isothermal Treatments at 210°C (Schedule 1)

Time at 210°C (Mins)	0.2% Offset yield strength		Ultimate Tensile Strength		Apparent Fracture Toughness $K_{app}$		Calculated Plane Strain Fracture Toughness		Hardness $R_c$
	ksi	MPa	ksi	MPa	ksi-in <sup>1/2</sup>	MPa-m <sup>1/2</sup>	ksi-in <sup>1/2</sup>	MPa-m <sup>1/2</sup>	
60	284.187	1959.6	331.551	2286.33	110.071	119.97	92.5	100.82	59.75
120	259.574	1721.0	321.098	2214.2	107.10	116.73	89	97.01	59.5
180	250.096	1724.5	312.241	2153.1	104.6	114.01	86.9	94.72	58.5
Martensitic:									
0	284.187	1959.6	333.079	2296.8	103.537	112.84	83	90.47	60

Isothermal Treatments at 210°C for 60 mins. - different tempering temps

Tempering Temp (°C)	0.2% Offset Yield Strength		Ultimate Tensile Strength		Apparent Fracture Toughness		Calculated Plane Strain Fracture Toughness		Hardness $R_c$
	ksi	MPa	ksi	MPa	ksi-in <sup>1/2</sup>	MPa-m <sup>1/2</sup>	ksi-in <sup>1/2</sup>	MPa-m <sup>1/2</sup>	
P.T.	165.01	1137.81	241.4	1664.5	65.59	71.49	48.74	53.12	57.6
400°C	242.5	1672.1	309.2	2132.07	93.24	101.63	73.54	80.15	56
650°C	183.2	1263.2	215.8	1488	45.57	49.67	28.17	30.70	45.5

Table III. Isothermal Treatments at 250°C (Schedule I)

Time at 250°C (mins)	0.2% Offset yield strength		Ultimate Tensile Strength		Apparent Fracture Toughness $K_{app}$		Calculated Plane Strain Fracture Toughness		Hardness $R_c$
	ksi	MPa	ksi	MPa	ksi-in <sup>1/2</sup>	MPa-m <sup>1/2</sup>	ksi-in <sup>1/2</sup>	MPa-m <sup>1/2</sup>	
60	242.78	1674.0	309.27	2132.5	52.55	57.28	25.59	27.29	58.4
120	218.26	1505	291.02	2006.7	48.80	53.19	23.33	25.42	58.4
180	231.31	1594.9	290.71	2004.5	47.64	51.92	22.03	24.01	58

Isothermal Treatments at 250°C for 60 mins. - Different Tempering Temps.

Tempering Temp (°C)	0.2% Offset Yield Strength		Ultimate Tensile Strength		Apparent Fracture Toughness		Calculated Plane Strain Fracture Toughness		Hardness $R_c$
	ksi	MPa	ksi	MPa	ksi-in <sup>1/2</sup>	MPa-m <sup>1/2</sup>	ksi-in <sup>1/2</sup>	MPa-m <sup>1/2</sup>	
R.T.	144.57	997.15	281.53	1941.6	5.56	6.06	-	-	56.3
400	195.56	1348.8	278.07	1917.4	23.51	27.57	4.23	4.61	54
650	184.91	1275.3	222.81	1536.7	12.58	13.71	10.53	11.44	46

Table IV. Schedule 2A

Tempering Temp. (°C)	0.2% Offset Yield Strength		Ultimate Tensile Strength		Apparent Fracture Toughness		Calculated Plane Strain Fracture Toughness		Hardness R <sub>c</sub>
	ksi	MPa	ksi	MPa	ksi-in <sup>1/2</sup>	MPa-m <sup>1/2</sup>	ksi-in <sup>1/2</sup>	MPa-m <sup>1/2</sup>	
550	183	1262.2	201	1386.3	68.23	74.37	50.15	54.66	46.7
400	190.9	1316.7	233.7	1611.9	79.82	86.98	67.11	73.14	45.5
300	181	1248.4	230	1586.4	67.39	73.45	52.33	57.04	33.6
210	143.6	990.4	227.6	1569.8	64.85	70.68	65.85	71.7	50.4

Table V. Schedule 2B

Isothermal Temperature and (time)	(0.2% Offset) Yield Strength		Ultimate Tensile Strength		Apparent Fracture Toughness K <sub>app</sub>		Calculated Plane Strain Fracture Toughness		Hardness R <sub>c</sub>
	ksi	MPa	ksi	MPa	ksi-in <sup>1/2</sup>	MPa-m <sup>1/2</sup>	ksi-in <sup>1/2</sup>	MPa-m <sup>1/2</sup>	
50°C	161.95	1117.03	201.68	1391	66.83	72.84	55.3	60.33	41.5
210°C (1hr)	152.02	1048.4	203.2	1401.5	65.59	71.49	53.69	58.52	43
210°C (2hr)	168.06	1159.17	224.09	1545.6	66.42	72.34	51.97	56.64	47
250°C (1hr)	134.45	927	198.62	1369.9	70.54	76.88	60.51	65.9	44
250°C (2hr)	152.78	1053.78	197.09	1358.7	71.78	78.24	62.3	67.9	41
Fully Bainitic:									
250°C (30hr)	148.20	1022.19	198.62	1369.9	63.74	69.47	52.01	56.69	43.5

Table VI. Fully Martensitic Structure vs. Fully Bainitic Structure - Tempered at 550°C (2hrs).

	(0.2% Offset) yield strength		Ultimate Tensile Strength		Apparent Fracture Toughness ( $K_{app}$ )		Calculated Plane Strain Fracture Toughness ( $K_{IC}$ )		Hardness $R_c$
	ksi	MPa	ksi	MPa	ksi-in <sup>1/2</sup>	MPa-m <sup>1/2</sup>	ksi-in <sup>1/2</sup>	MPa-m <sup>1/2</sup>	
Fully Martensitic	153	1262.2	201	1386.3	68.23	74.37	50.15	54.66	46.7
Fully Bainitic	133.2	1022.19	198.62	1369.9	63.74	69.47	52.01	56.69	43.5

FIGURE CAPTIONS

- Fig. 1. Theta dilatometer used for obtaining TTT diagram data.
- Fig. 2. Time-temperature-transformation diagram of Vasco MA (in the lower bainite range) showing start of transformation (1%) and finish (99%) transformation.
- Fig. 3. Set-up used for heat-treatments.
- Fig. 4. Round tensile specimen.
- Fig. 5. Three point bend test specimen.
- Fig. 6. Set-up used for three-point bend testing showing MTS, test-specimen and crack-opening displacement gage.
- Fig. 7. Photomicrograph showing undissolved carbides present near prior austenite grain boundaries, after 1100°C austenitization treatment (Specimen H-8).
- Fig. 8. Heat treatment schedule I.
- Fig. 9. Hardness versus tempering temperature curve of duplex microstructure (martensite + lower bainite) produced after 1 hour isothermal treatment at 210°C.
- Fig. 10. Yield and ultimate tensile strengths versus isothermal treatment time (at 210°C) for duplex structures. Specimens tempered at 550°C (2 hrs.).
- Fig. 11. Hardness vs. isothermal treatment time (210°/250°C).
- Fig. 12. Strength versus tempering temperature curves for duplex microstructures produced after 1 hr. isothermal transformation at (210°/250°C).

- Fig. 13. Hardness vs. tempering temperature curve of the duplex microstructure (martensite + bainite) produced after 1 hour isothermal treatment at 250°C.
- Fig. 14. Calculated plane strain fracture toughness ( $K_{Ic}$ ) versus isothermal transformation time for duplex microstructures produced after isothermal treatment at (210°/250°C).
- Fig. 15. (a) Scanning electron fractograph of three-point bend specimen, subjected to isothermal transformation at 210°C (2 hrs.) plus tempering at 550°C (2 hrs.). The fracture mode is primarily dimpled rupture.  
(b) Enlarged view of fracture surface of specimen in 15(a).  
(c) Optical micrograph of specimen 32, subjected to isothermal transformation at 210°C (2 hrs.).
- Fig. 16. (a) Fracture surface of three point-bend specimen, subjected to isothermal transformation at 210°C (3 hrs.), plus tempering at 550°C (2 hrs.). The mode of fracture appears to be quasi-cleavage.  
(b) Optical micrograph of three point-bend specimen in 16(a).
- Fig. 17. (a) Fracture surface of three-point bend specimen subjected to isothermal transformation at 250°C (1 hr) plus tempering at 550°C (2 hrs) - Quasi-cleavage.  
(b) & (c) Optical micrographs showing carbides present in the matrix of specimens transformed isothermally at 250°C (1 hr).
- Fig. 18. (a) & (b) Duplex microstructures produced after 1 hr. isothermal transformation at 250°C, plus tempering at 400°C (2 hrs). Coarse carbides are present in the matrix.

Fig. 19. (a) Fracture surface of three-point bend specimen transformed isothermally at 250°C (2 hrs.) plus tempering at 550°C (2 hrs.). The fracture surface appears to show quasi-cleavage facets.

(b) Optical micrograph from dilatometer specimen, isothermally transformed at 250°C (2 hrs.) and quenched to room temperature (Duplex microstructure).

Fig. 20. Heat treatment schedules 2A and 2B. Schedule 2A refers to a thermal cycling austenitization treatment plus quench & temper. Schedule 2B refers to a thermal cycling austenitization treatment plus isothermal transformations followed by tempering.

Fig. 21. Strength and calculated plane strain fracture toughness versus tempering temperature curves for specimens subjected to Schedule 2A.

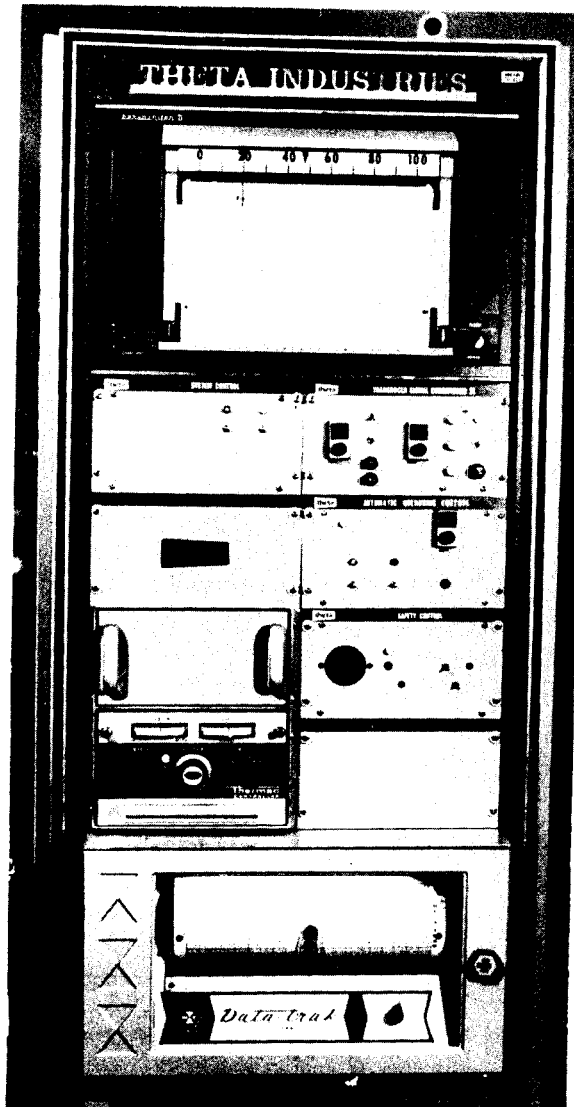
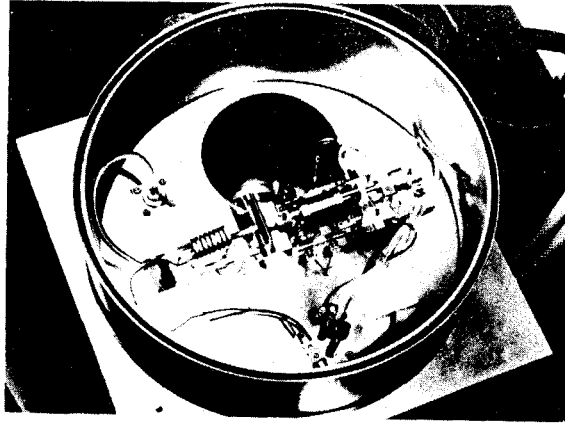
Fig. 22. Hardness versus tempering temperature curves for specimens subjected to Schedule 2A.

Fig. 23. Fracture surface of three point bend test specimen 302 subjected to Schedule 2A plus tempering at 550°C (2 hrs) essentially quasi-cleavage.

Fig. 24. Three point bend specimen subjected to schedule 2A Tempered at 400°C (2 hrs.). The fracture surfaces (a) & (c) are essentially quasi-cleavage. The optical micrograph in (b) shows a fine dispersion of carbides.

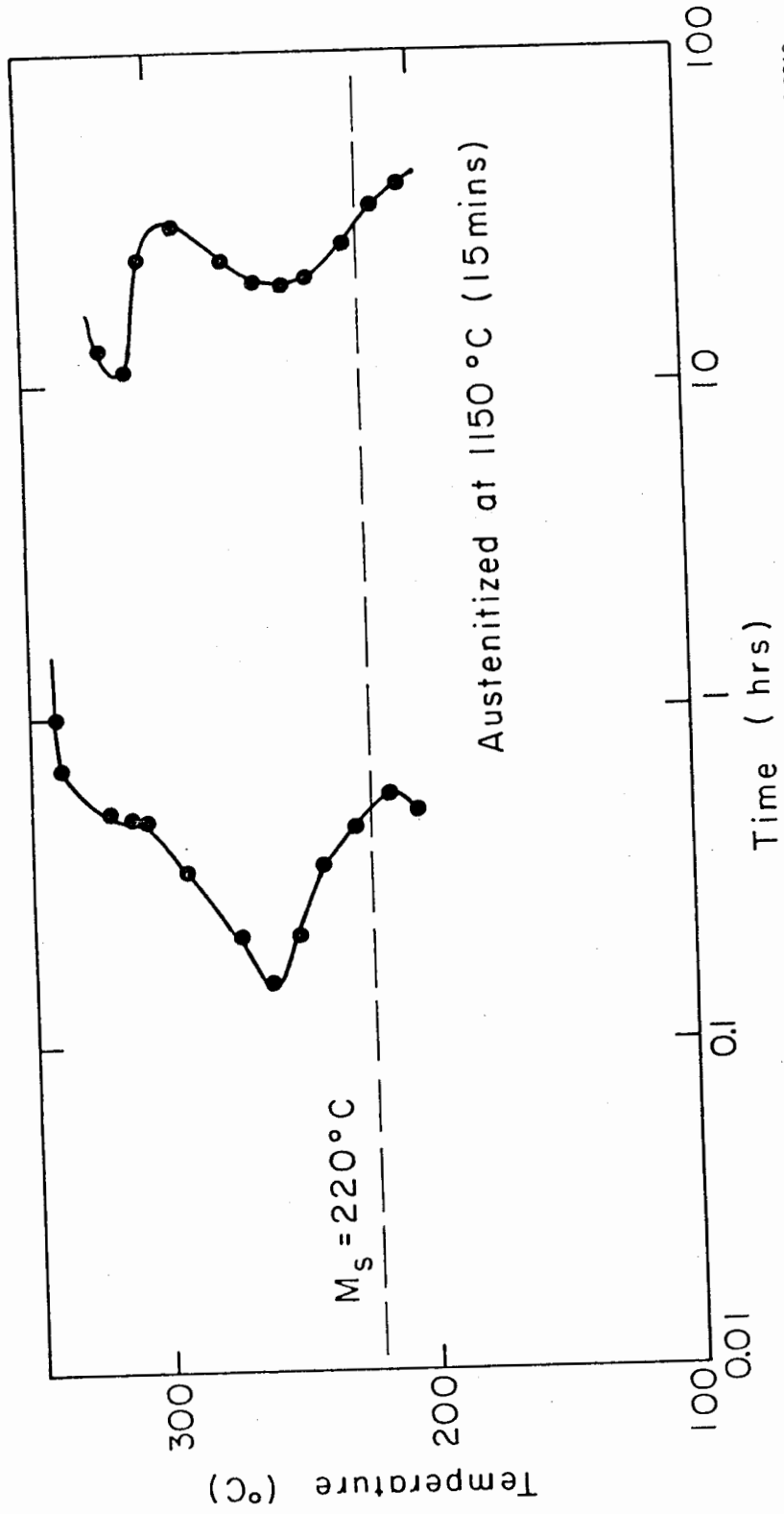
- Fig. 25. Three point bend specimen subjected to schedule 2A - tempered at 550°C (2 hrs.). (a) represents the microstructure obtained and (b) shows the fracture surface quasi-cleavage.
- Fig. 26. Curves showing strength and calculated plane strain fracture toughness versus isothermal treatment time at 210°C using schedule 2B<sub>1</sub>.
- Fig. 27. Curves showing strength and calculated plane strain fracture toughness versus isothermal treatment time at 250°C using schedule 2B<sub>2</sub>.
- Fig. 28. Optical micrograph showing microstructures obtained after isothermal transformation at 250°C for 30 hrs. (fully bainitic). (a) shows the prior austenite grain size and (b), (c) represent the microstructure.
- Fig. 29. Curves showing hardness vs. isothermal transformation time, for schedules 2B<sub>1</sub>, (210°C isothermal) & 2B<sub>2</sub> (250°C isothermal).
- Fig. 30. Curves showing strength and calculated K<sub>IC</sub> versus isothermal treatment time at 250°C using schedule 2B<sub>2</sub>.
- Fig. 31. (a) & (b) Fracture surfaces of specimens as in 30. The fracture mode is essentially quasi-cleavage.
- Fig. 32. Fracture surface of the fully bainitic structure, showing quasi-cleavage.
- Fig. 33. Effect of thermal cycling on the strength of the secondary hardening Vasco MO steel. Schedule 1 ≡ commercial austenitization; schedule 2B<sub>1</sub> ≡ thermal cycling.

- Fig. 34. Effect of thermal cycling on yield strength - calculated  $K_{Ic}$  of the secondary hardening Vasco MA steel. Schedule 1  $\equiv$  commercial austenitization; Schedule 2  $\equiv$  thermal cycling.
- Fig. 35. EDAX analysis of matrix and carbide of specimen H-8, subjected to commercial austenitization + quench and temper at 550°C (2 hrs.).
- Fig. 36. EDAX analysis of matrix and carbide of specimen subjected to thermal cycling + temper at 400°C (specimen 303) & temper at 550°C (specimen 302).
- Fig. 37. Visual display on the Edax showing the peaks for the various elements present.
- Fig. 38. Three carbides on a specimen tempered at 550°C (2 hrs.) which were analyzed on the EDAX.
- Fig. 39. EDAX analysis of carbides in 38.



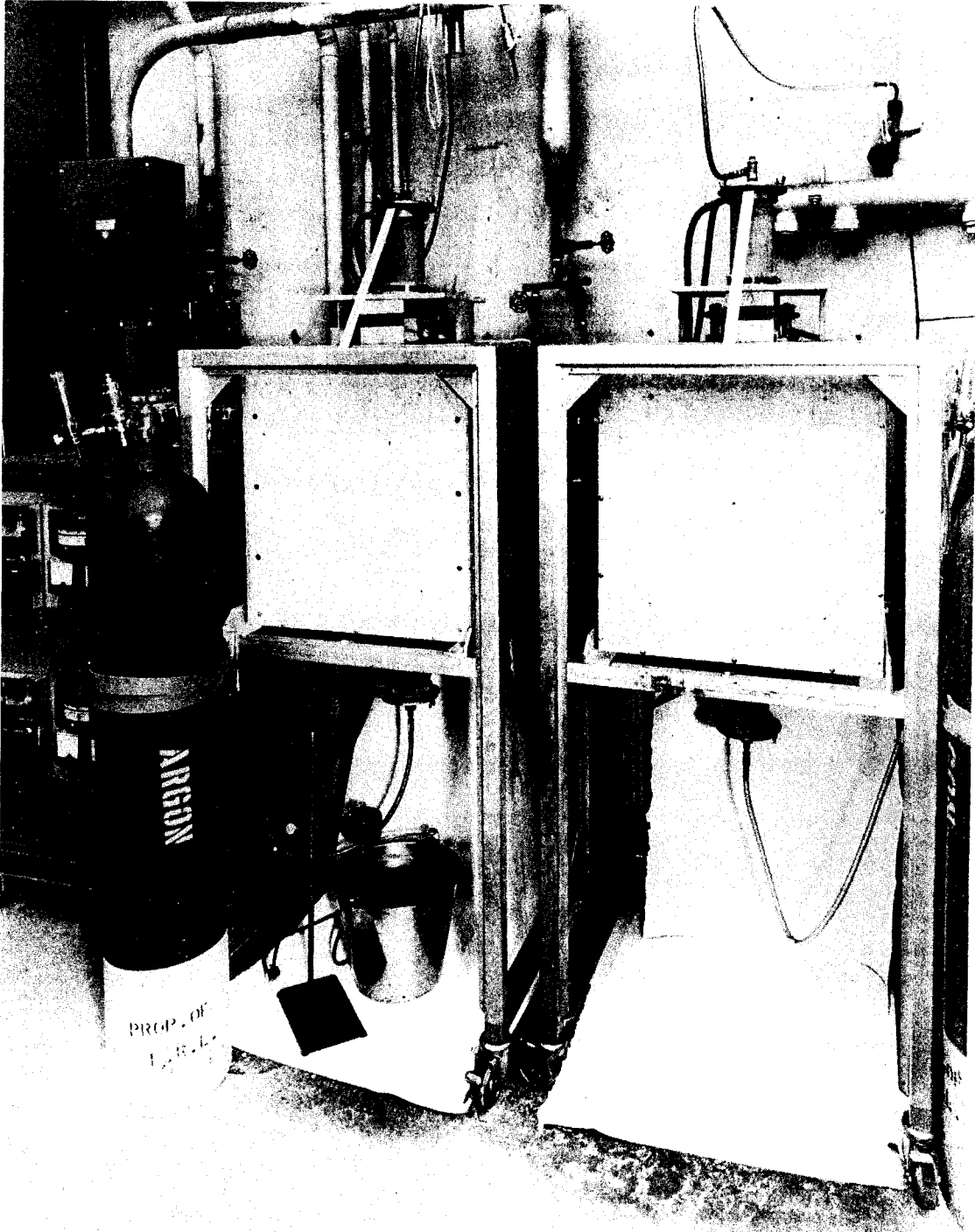
XBB 754-2369C

Fig. 1.



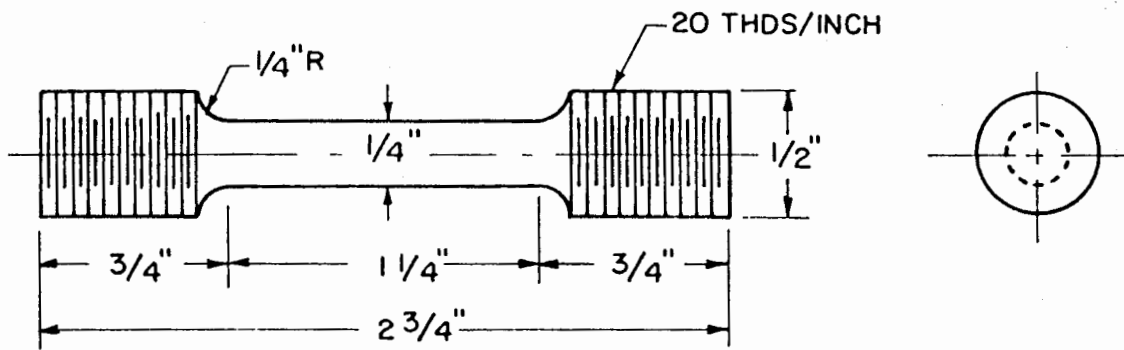
XBL 768-3310

FIG. 2.



XBB 732-504

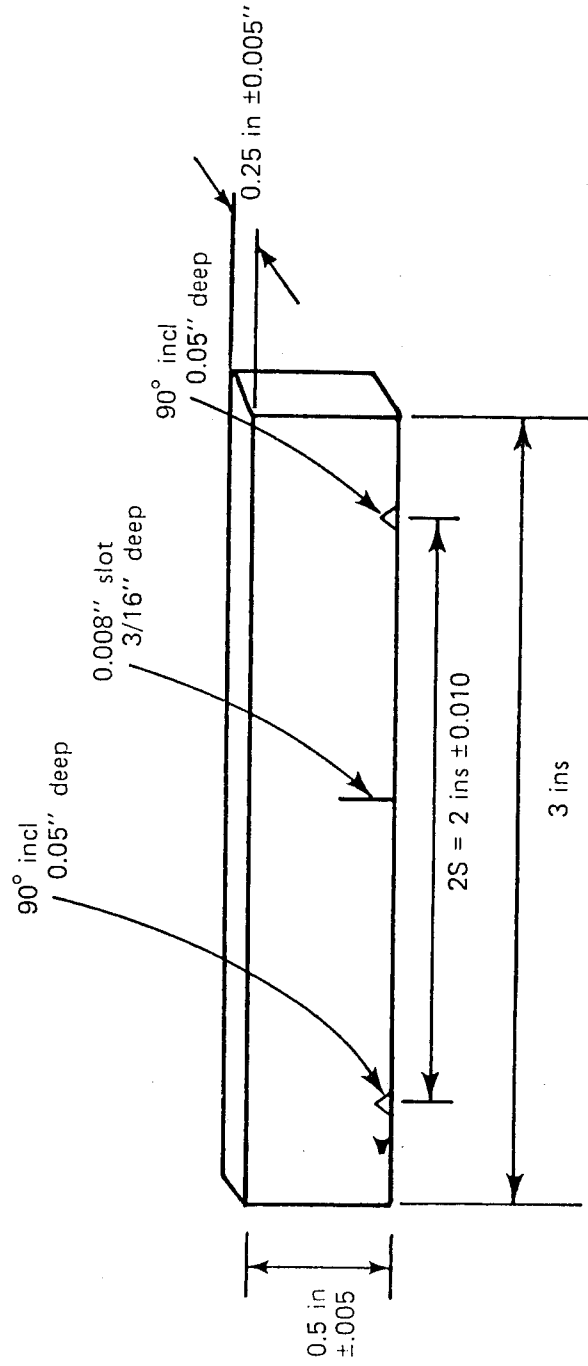
Fig. 3.



(b) ROUND TENSILE SPECIMEN

XBL 735-6189A

FIG. 4.



XBL 768-3300

Fig. 5.



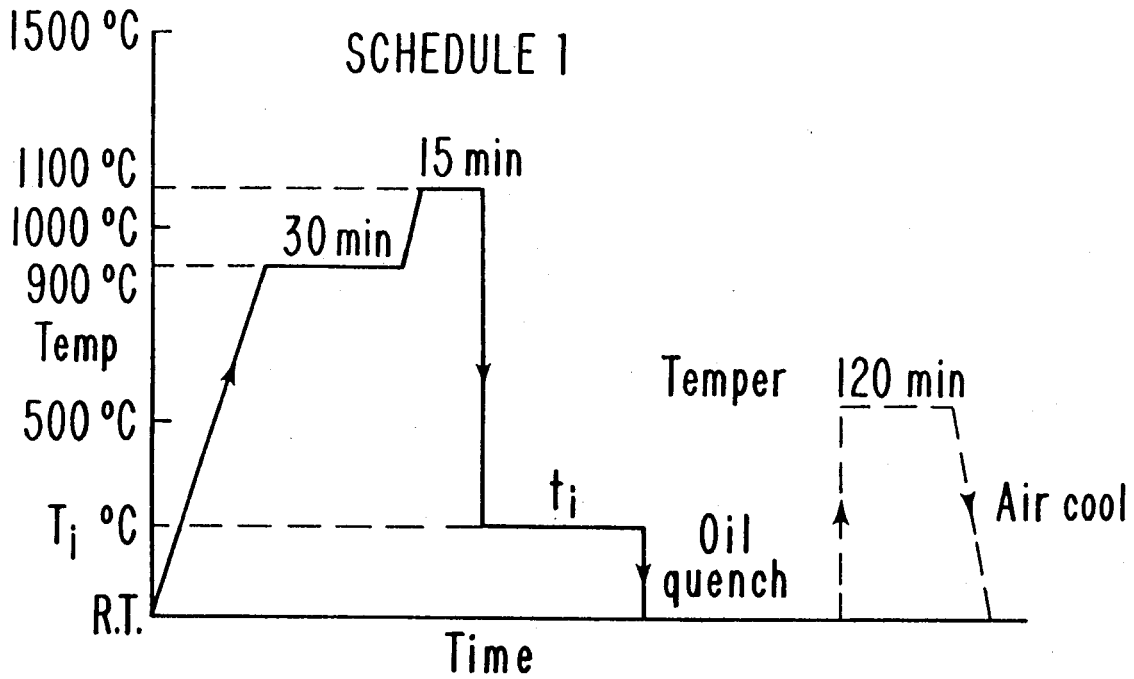
XBB 767-6740

Fig. 6.



XBB 768-7548

Fig. 7.

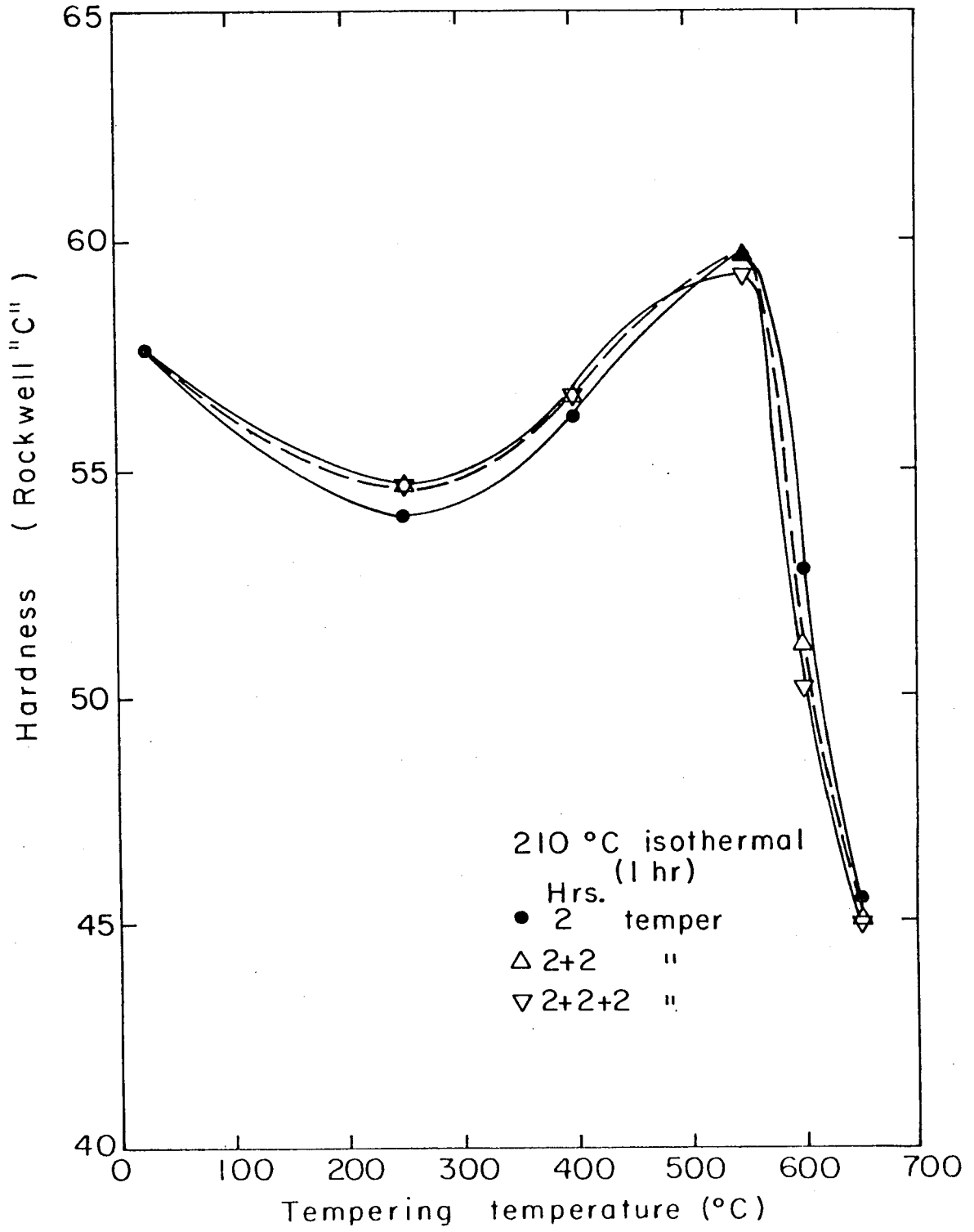


$T_i = 250^\circ\text{C} / 210^\circ\text{C}$

$t_i = 60 \text{ min} / 120 \text{ min} / 180 \text{ min}$

XBL 768-3253

Fig. 8.



XBL 768-3309

Fig. 9.

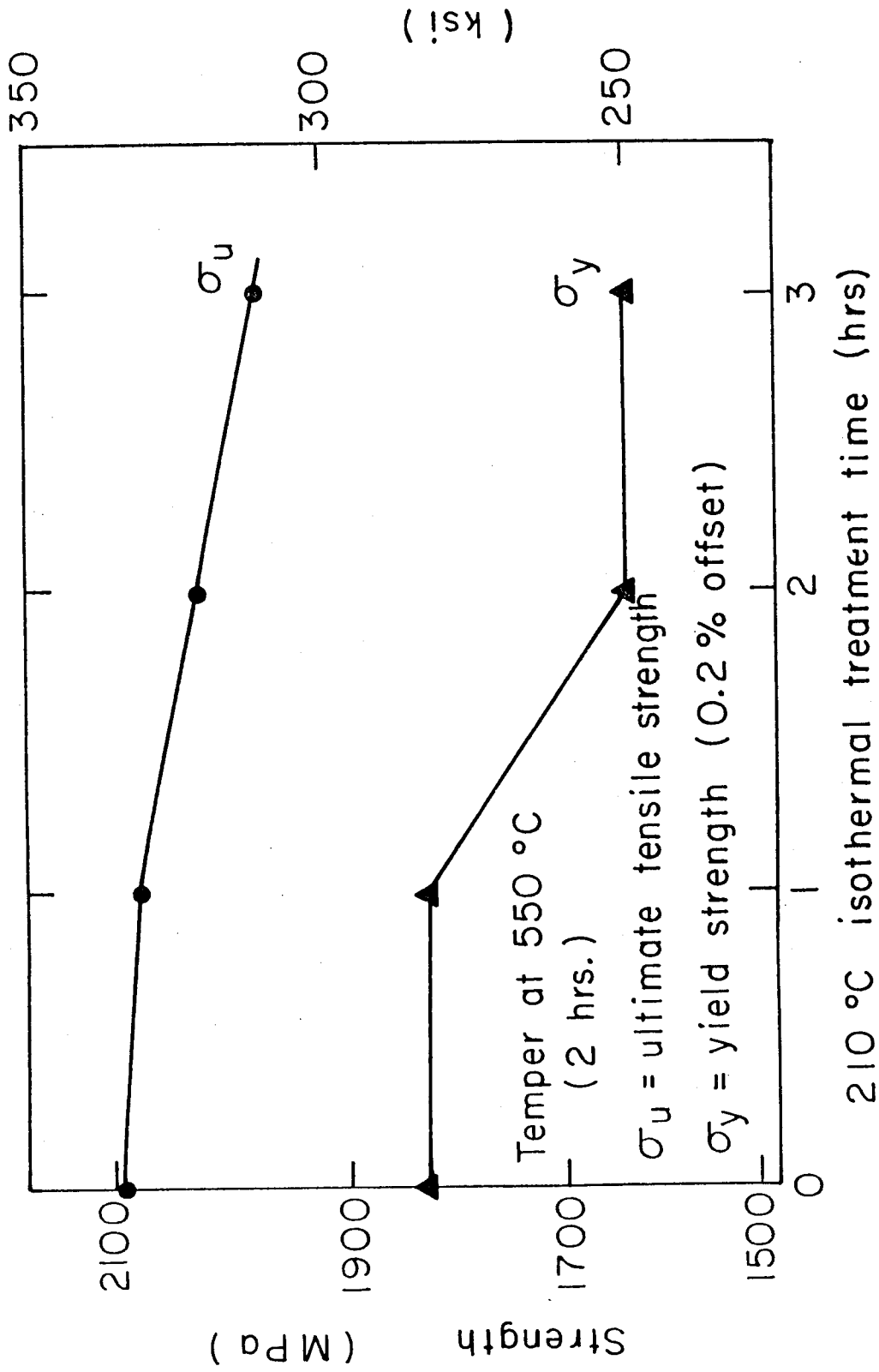


FIG. 10.

XBL 768-3317

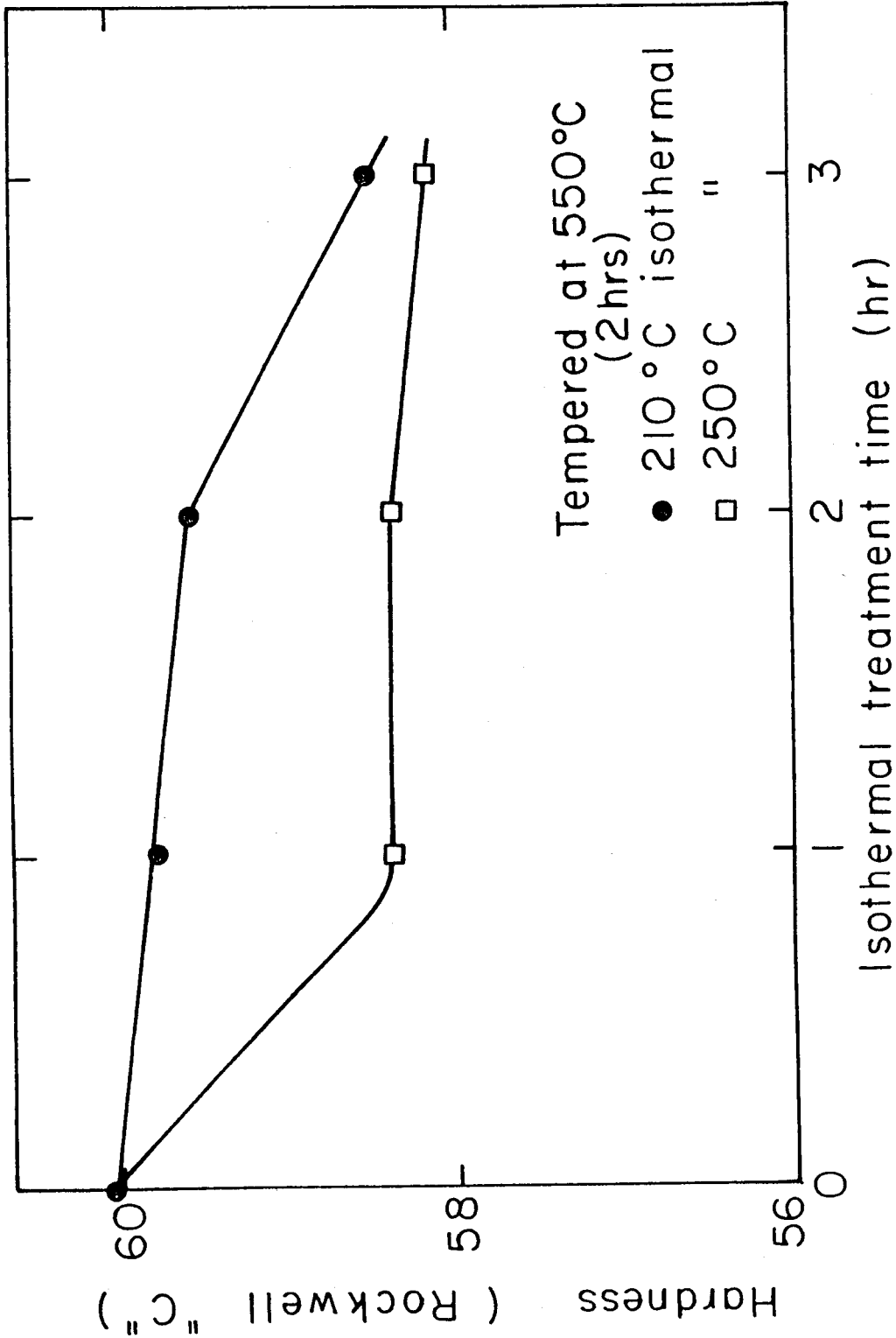
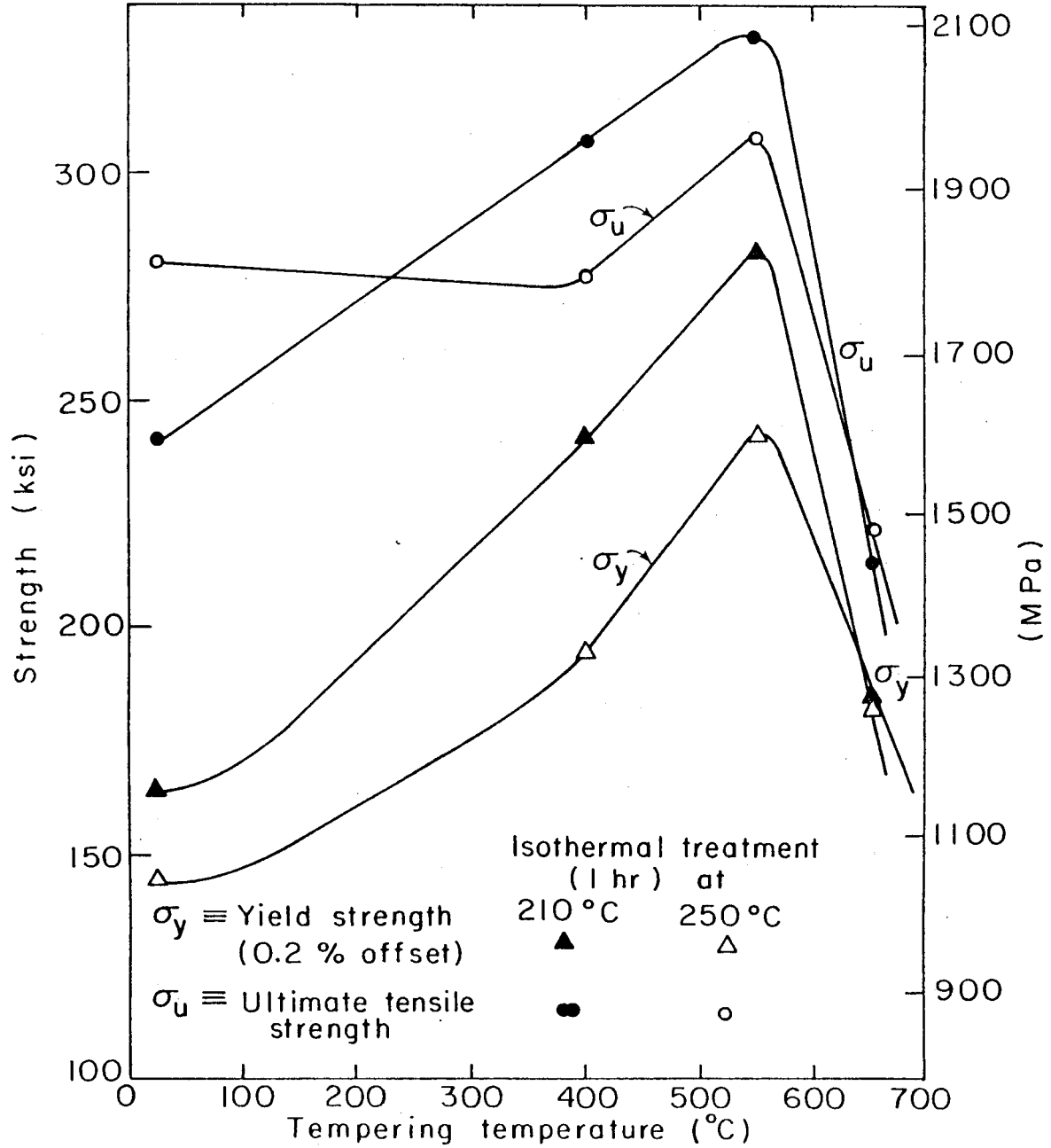


Fig. 11.

XBL 768-3311



XBL 768 3316

Fig. 12.

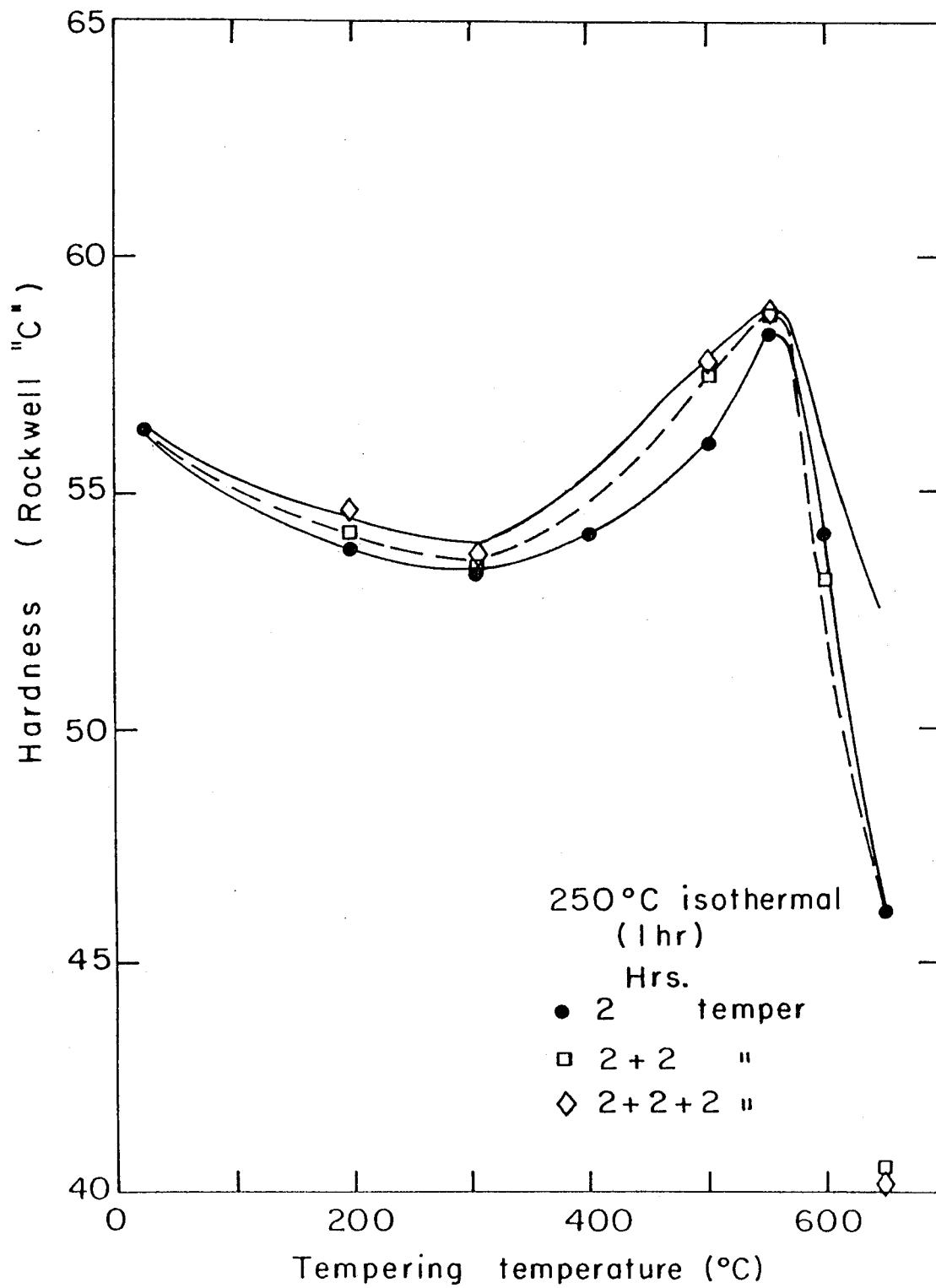
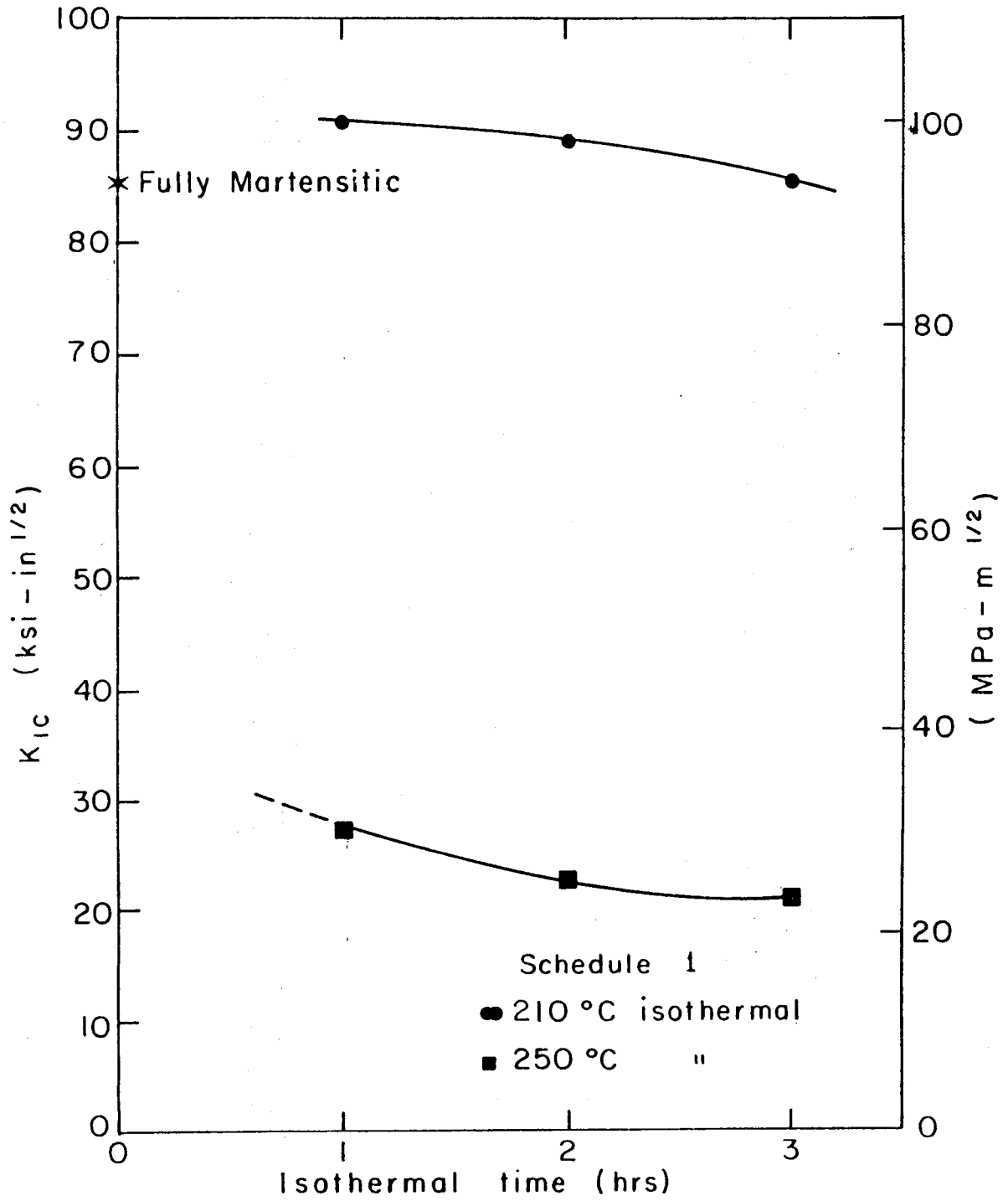


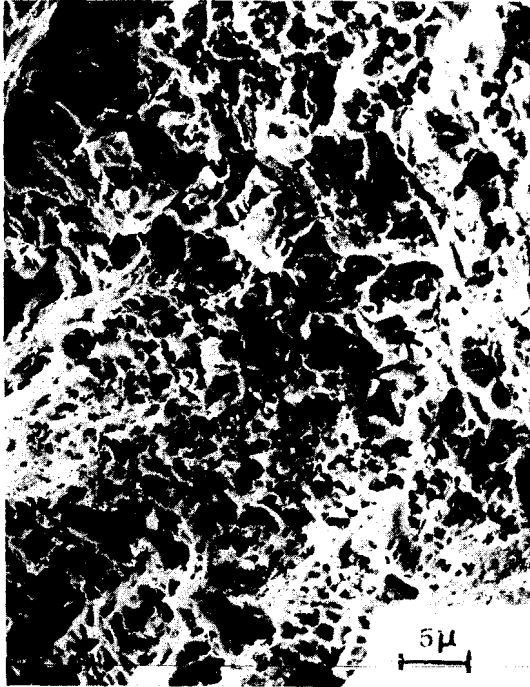
Fig. 13.

XBL 768-3320



XBL 768-3312

Fig. 14.



(a)

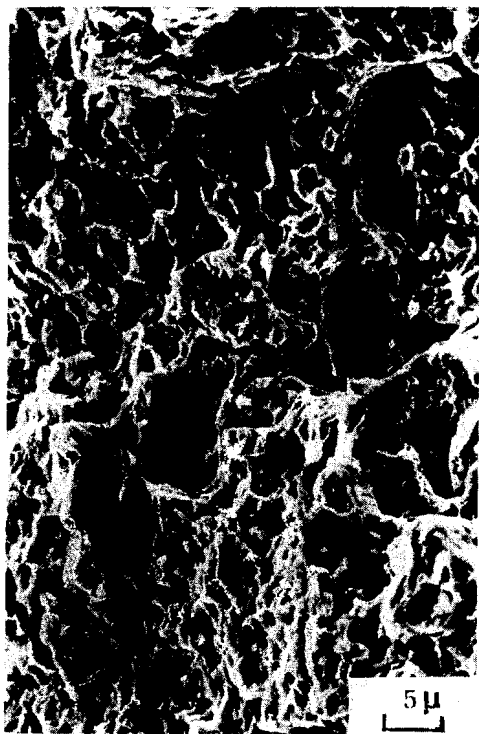


(c)

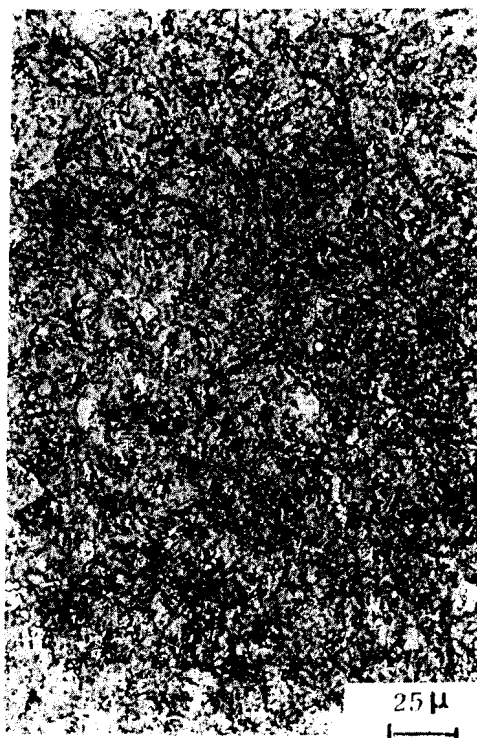


(b) XBB 768-7547

Fig. 15.



(a)

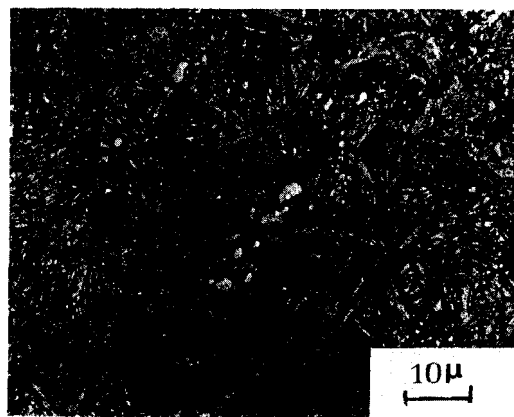


(b) XBB 768-7542

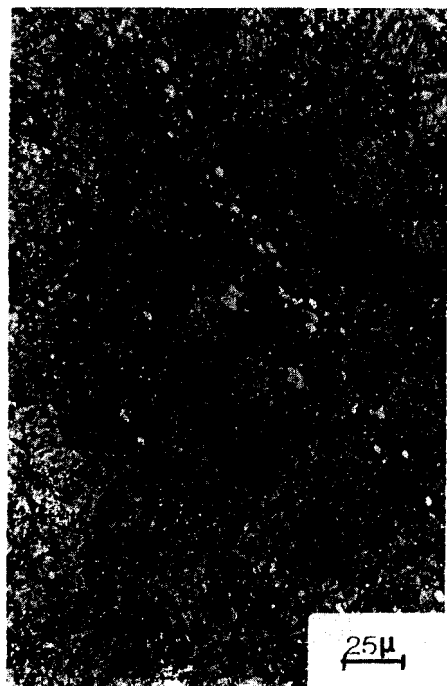
Fig. 16.



(a)



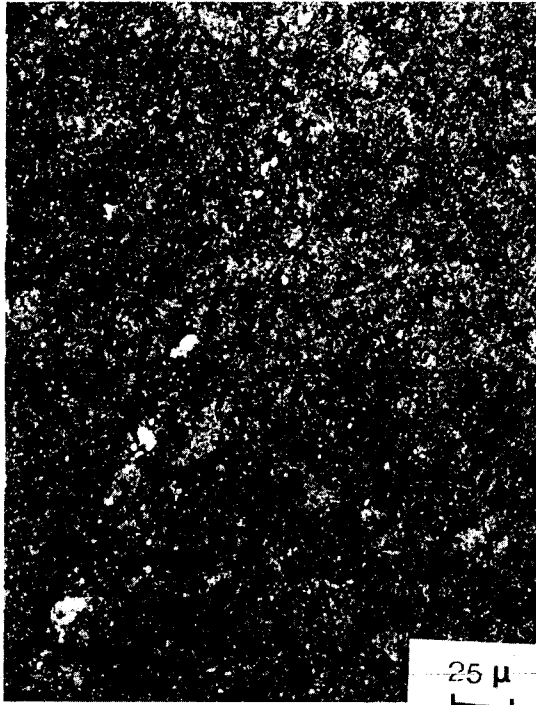
(b)



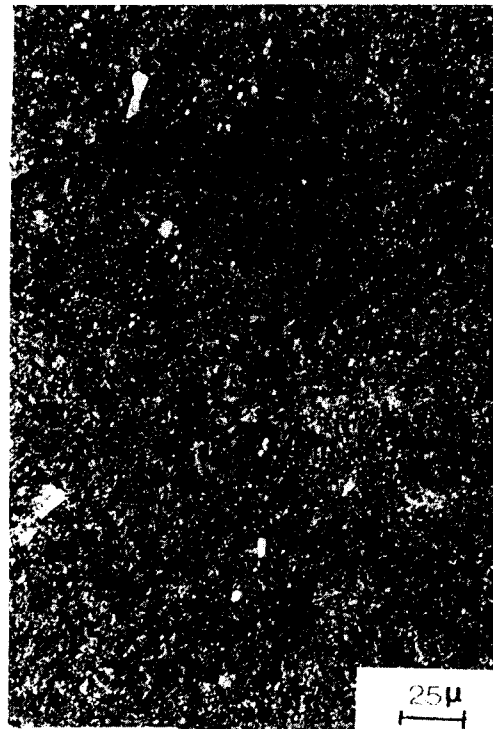
(c)

XBB 768-7546

Fig. 17.

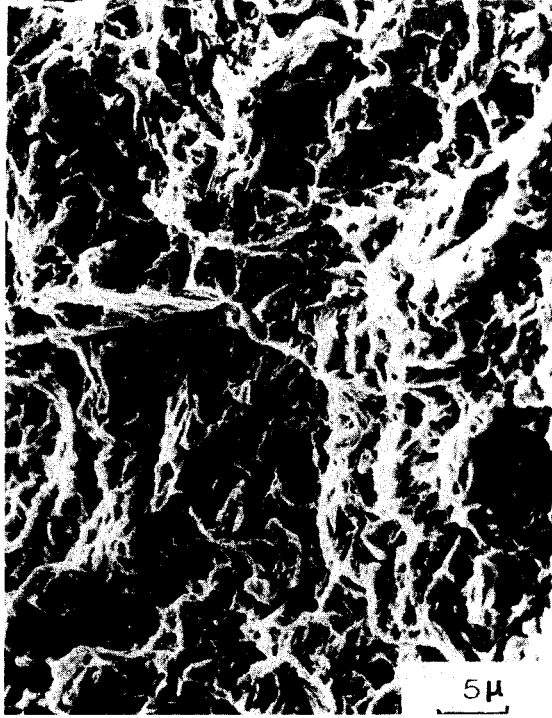


(a)



(b) XBB 768-7543

Fig. 18.



(a)



(b) XBB 768-7539

Fig. 19.

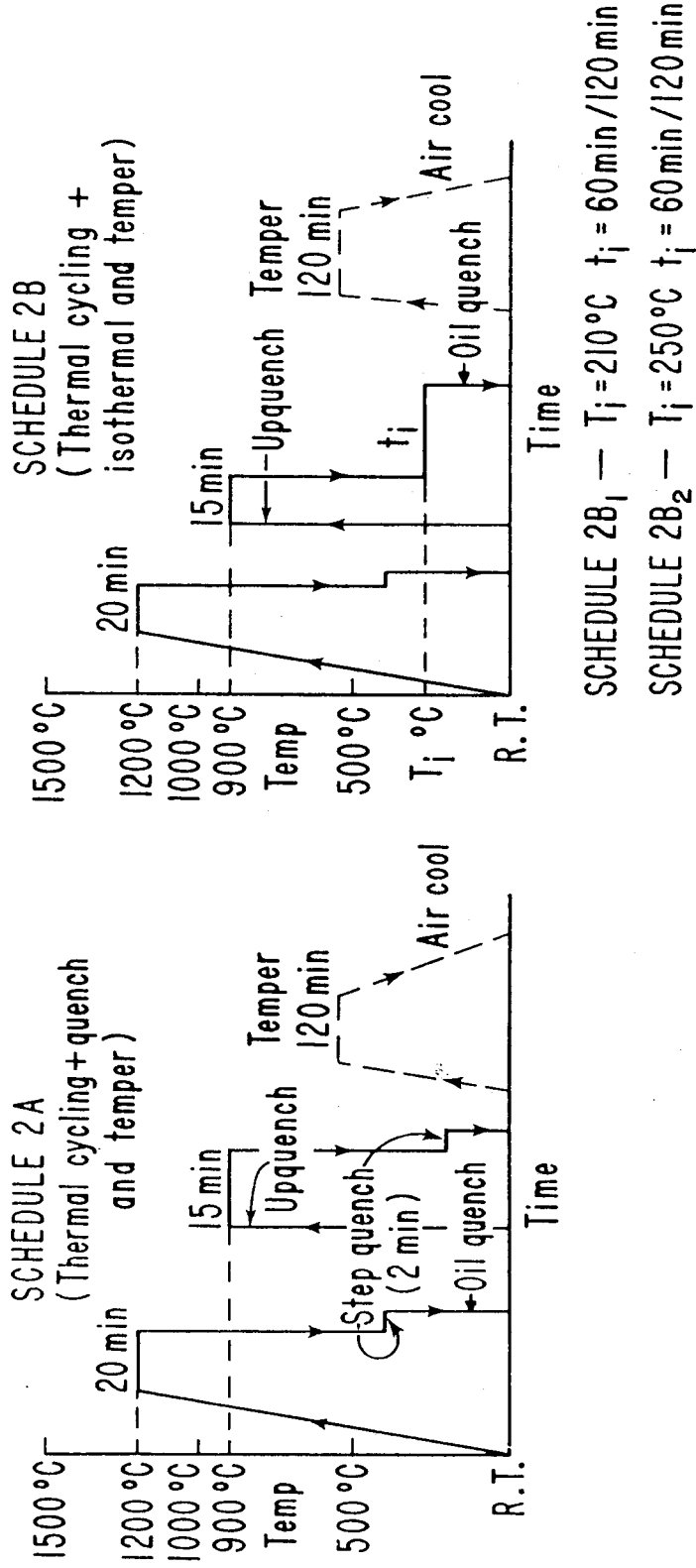
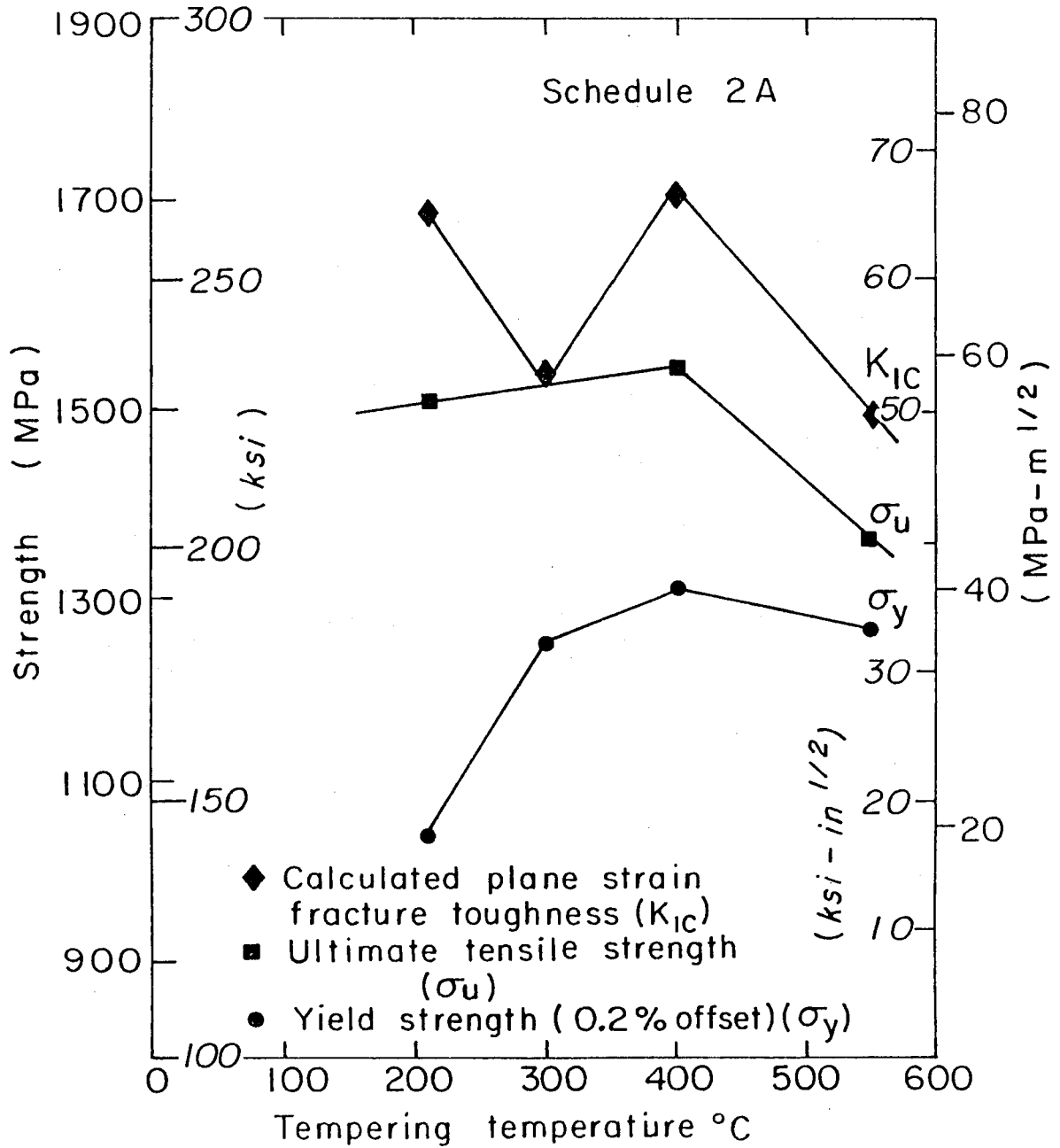


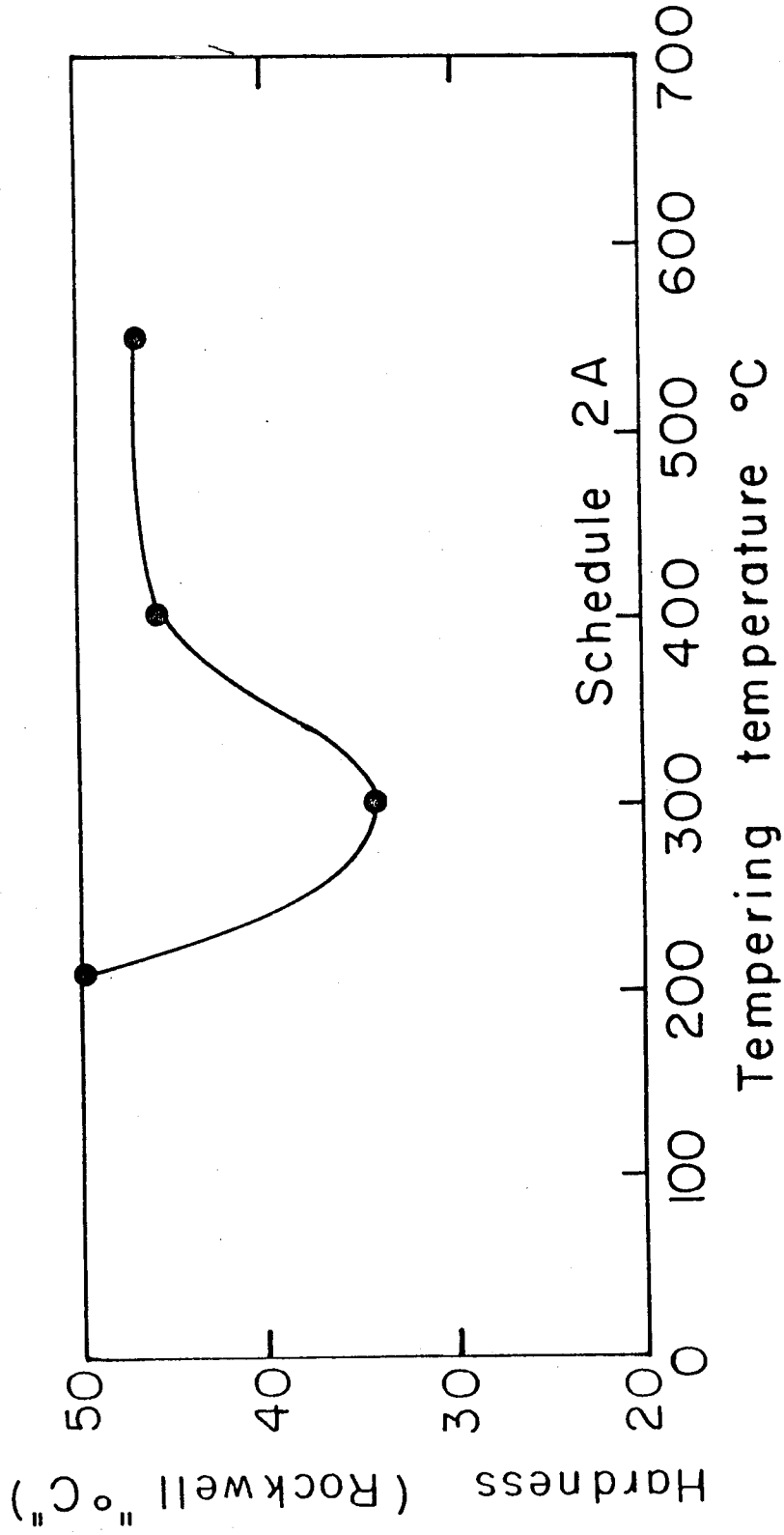
FIG. 20.

XBL 768 - 3254 - A



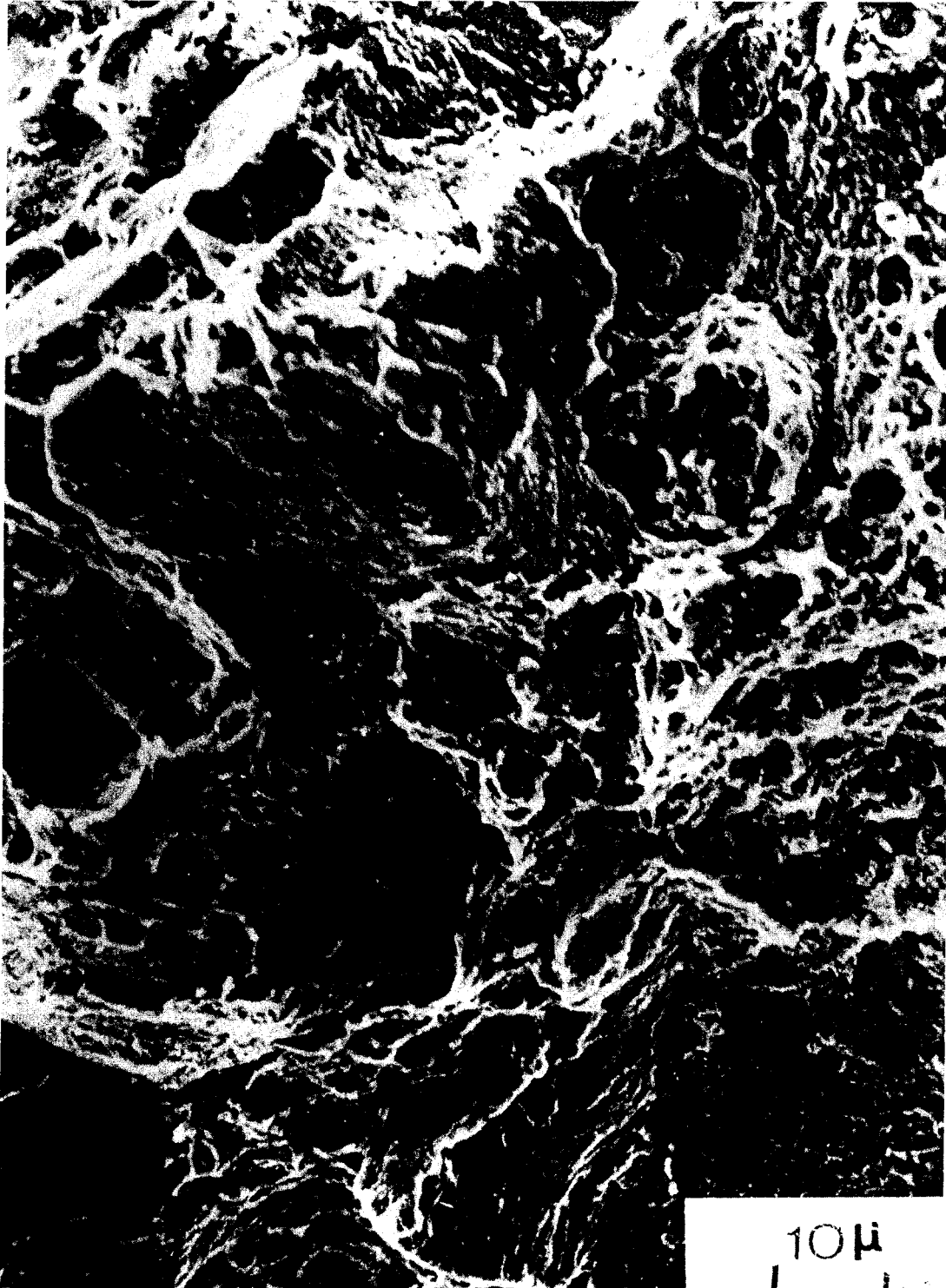
XBL 768 3318

Fig. 21.



XBL 768-3307

FIG. 22.

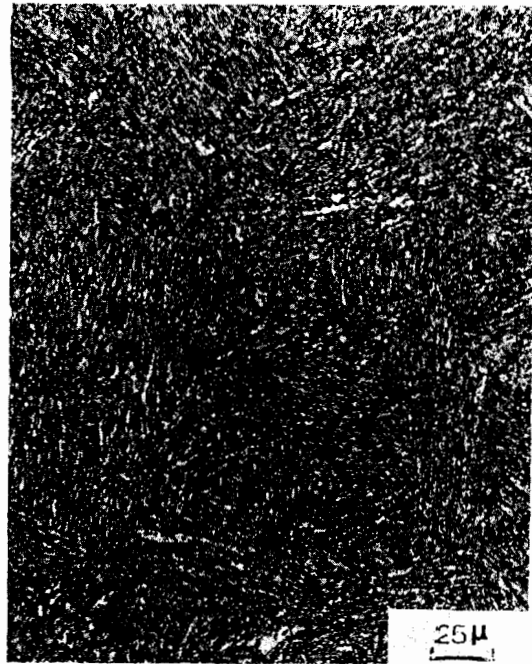


XBB 768-7538

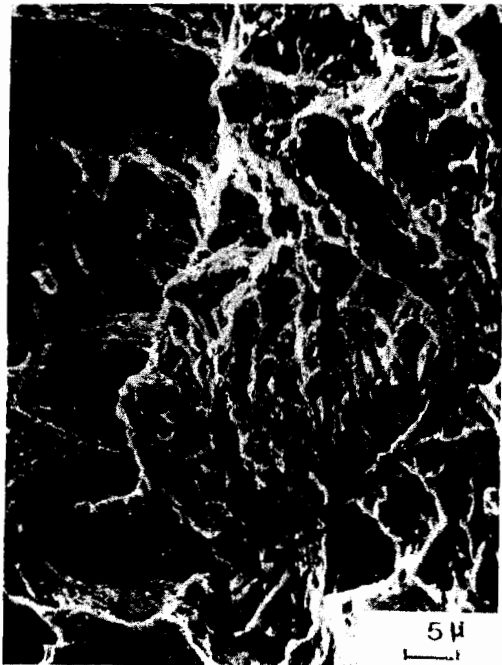
Fig. 23.



(a)



(b)



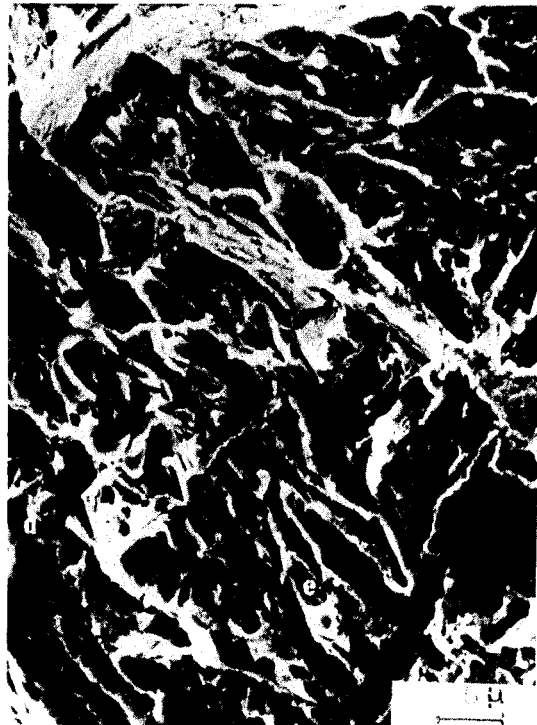
(c)

XBB 768-7544

Fig. 24.

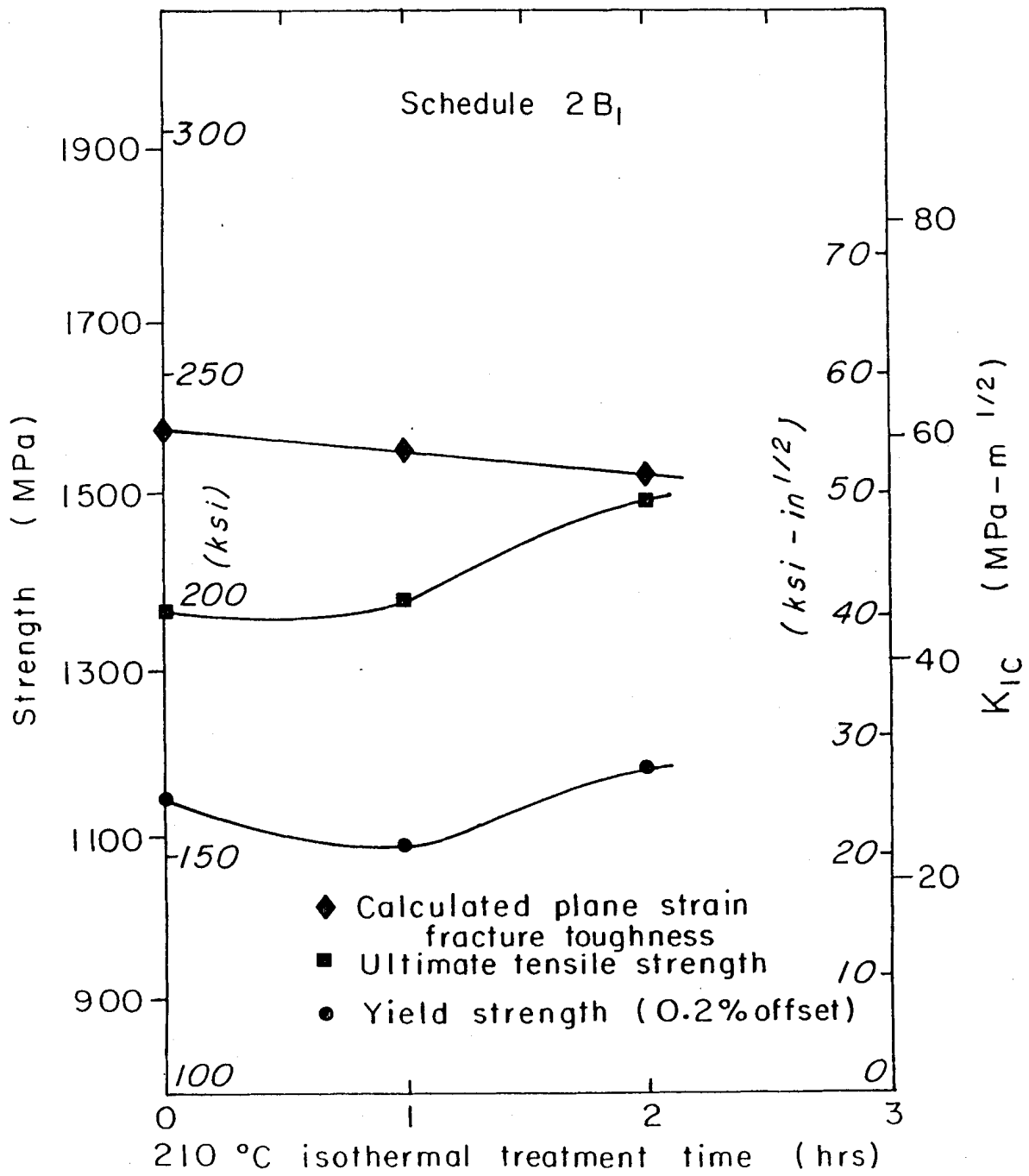


(a)



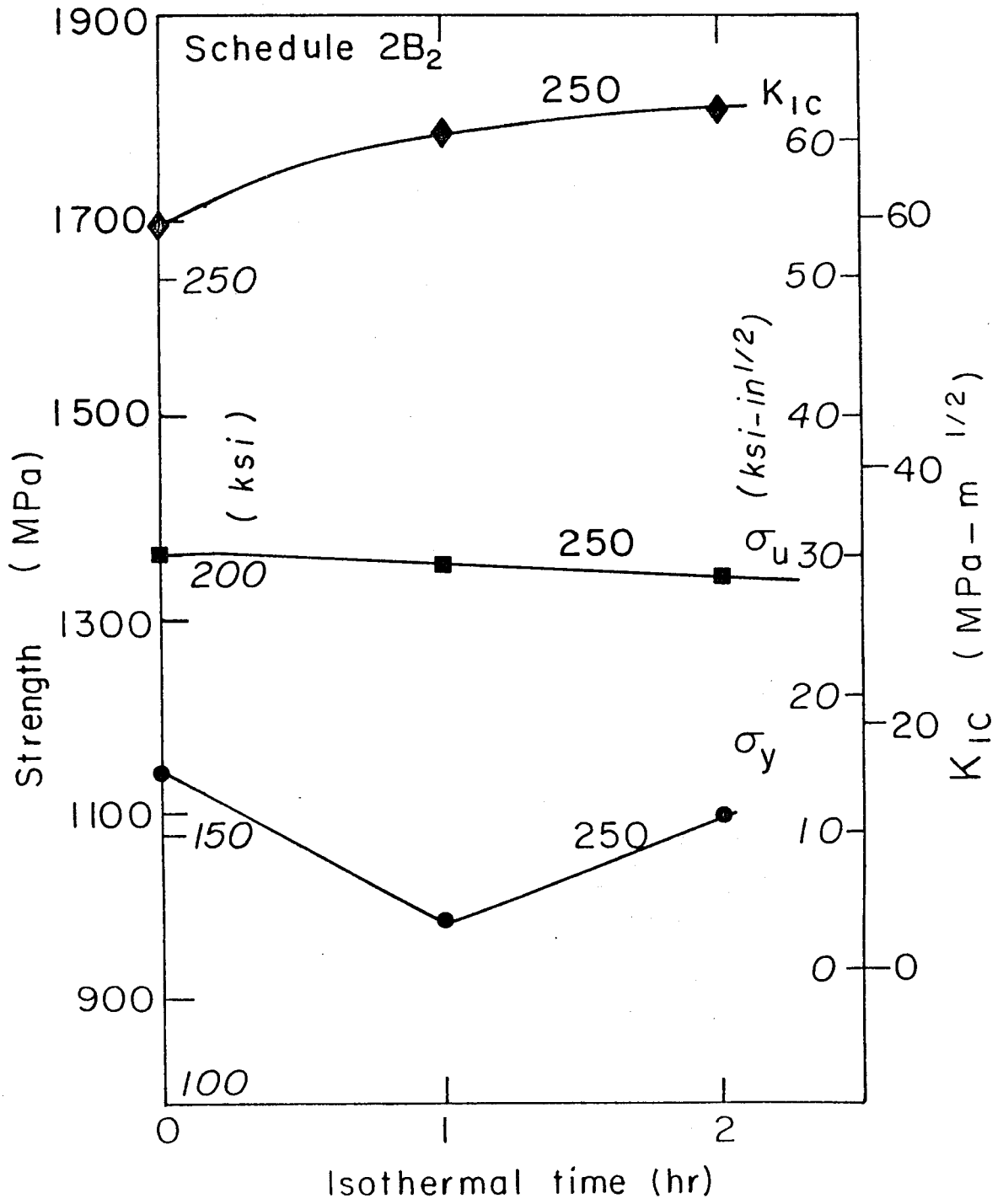
(b) XBB 768-754C

Fig. 25.



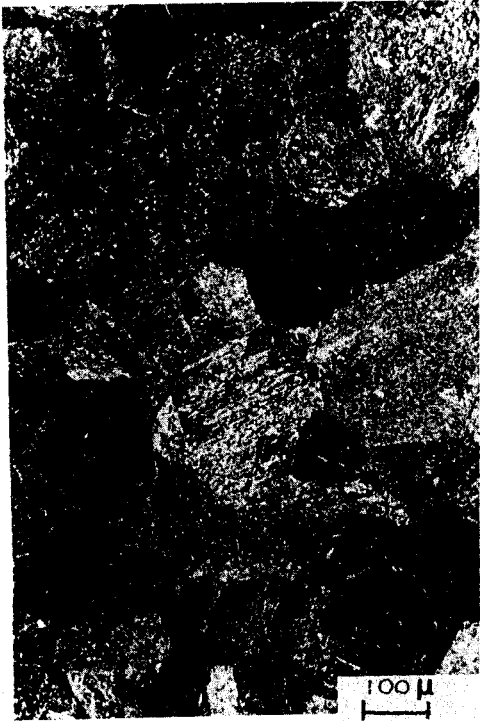
XBL 768-3322

Fig. 26.

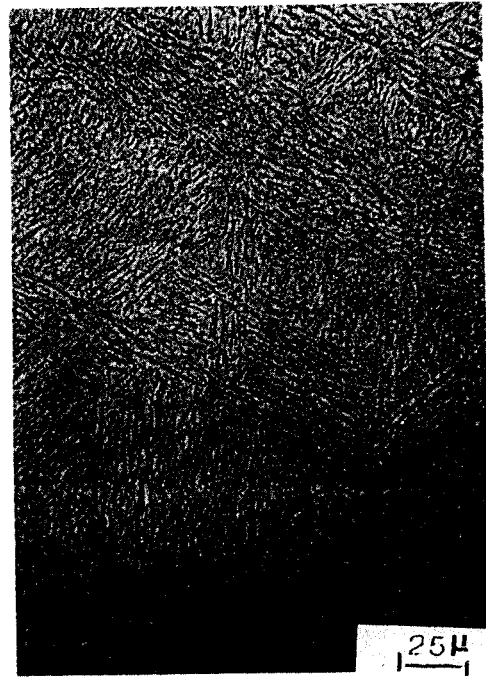


XBL 768-3319

Fig. 27.



(a)



(c)



(b)

XBB 768-7545

Fig. 28.

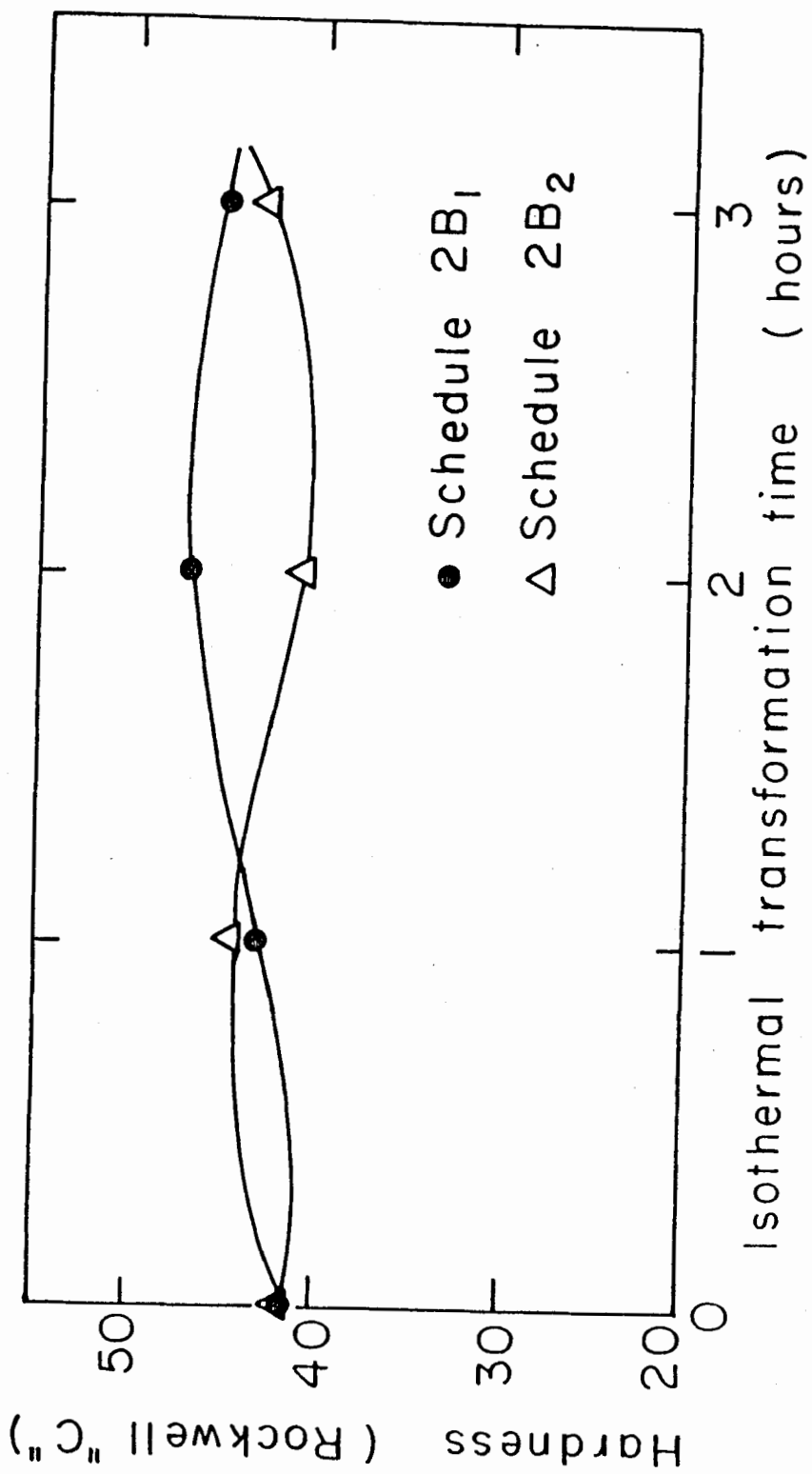
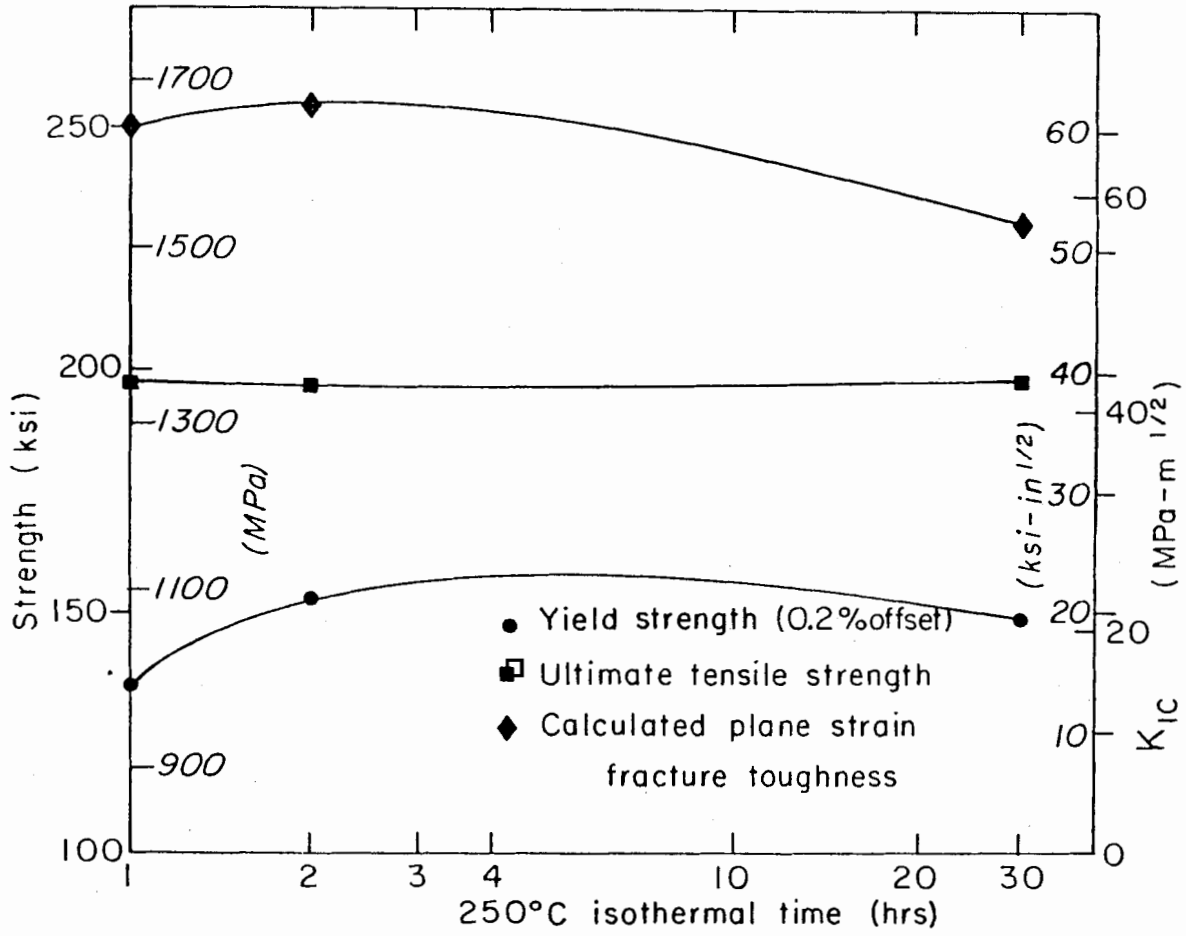


Fig. 29.

XBL 768-3305



XBL 768-3313

Fig. 30.

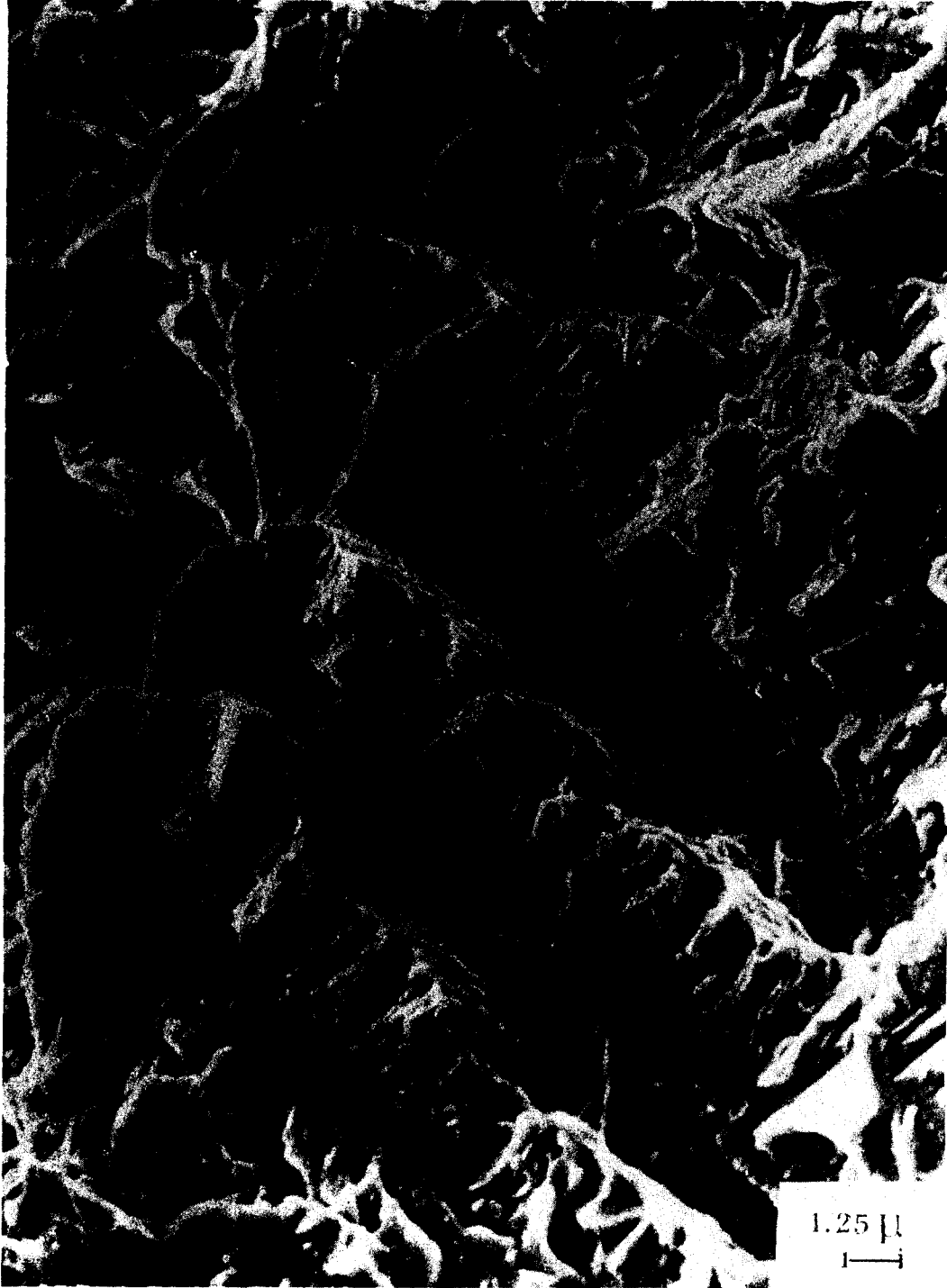


(a)



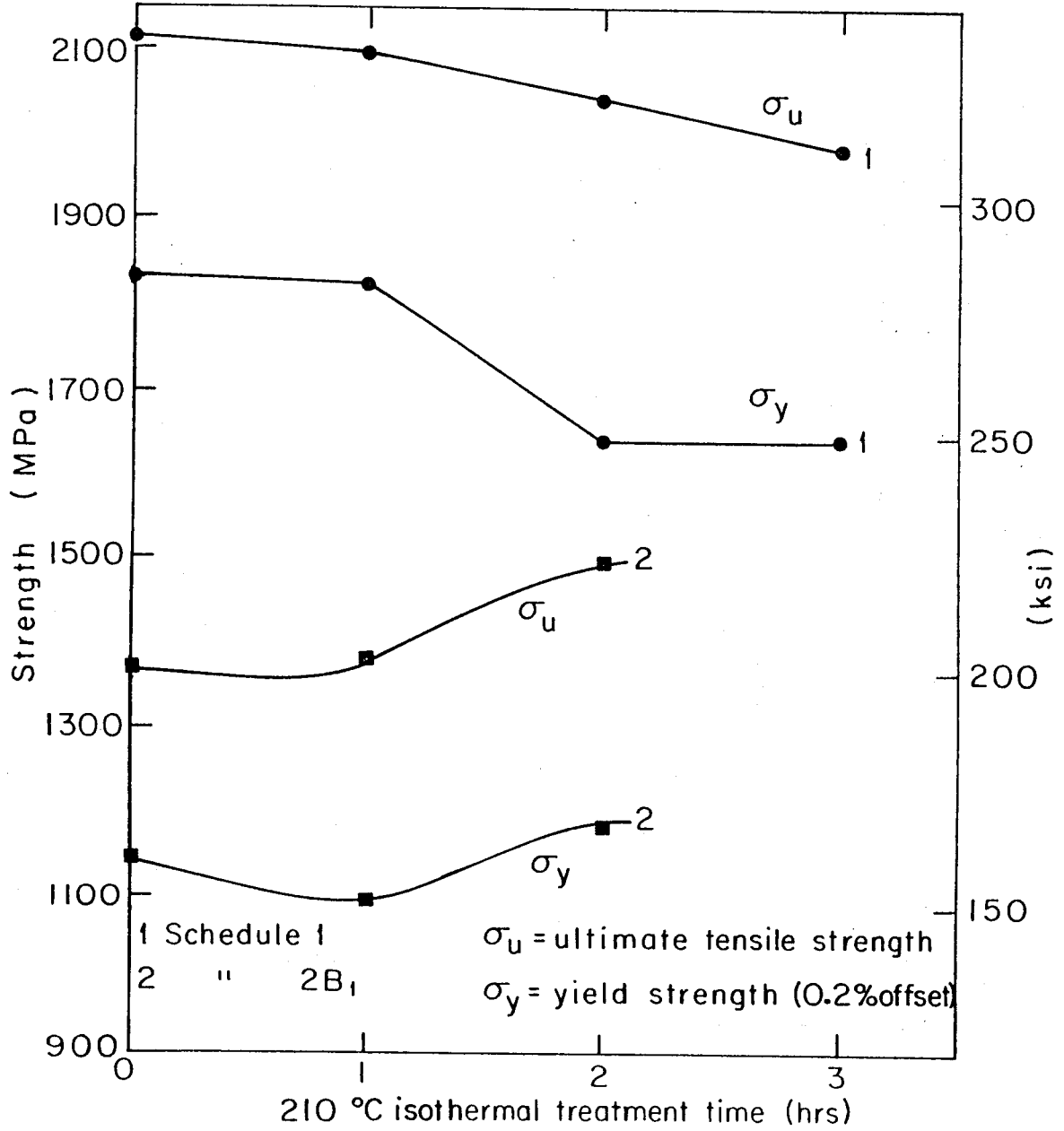
(b) XBB 768-7541

Fig. 31.



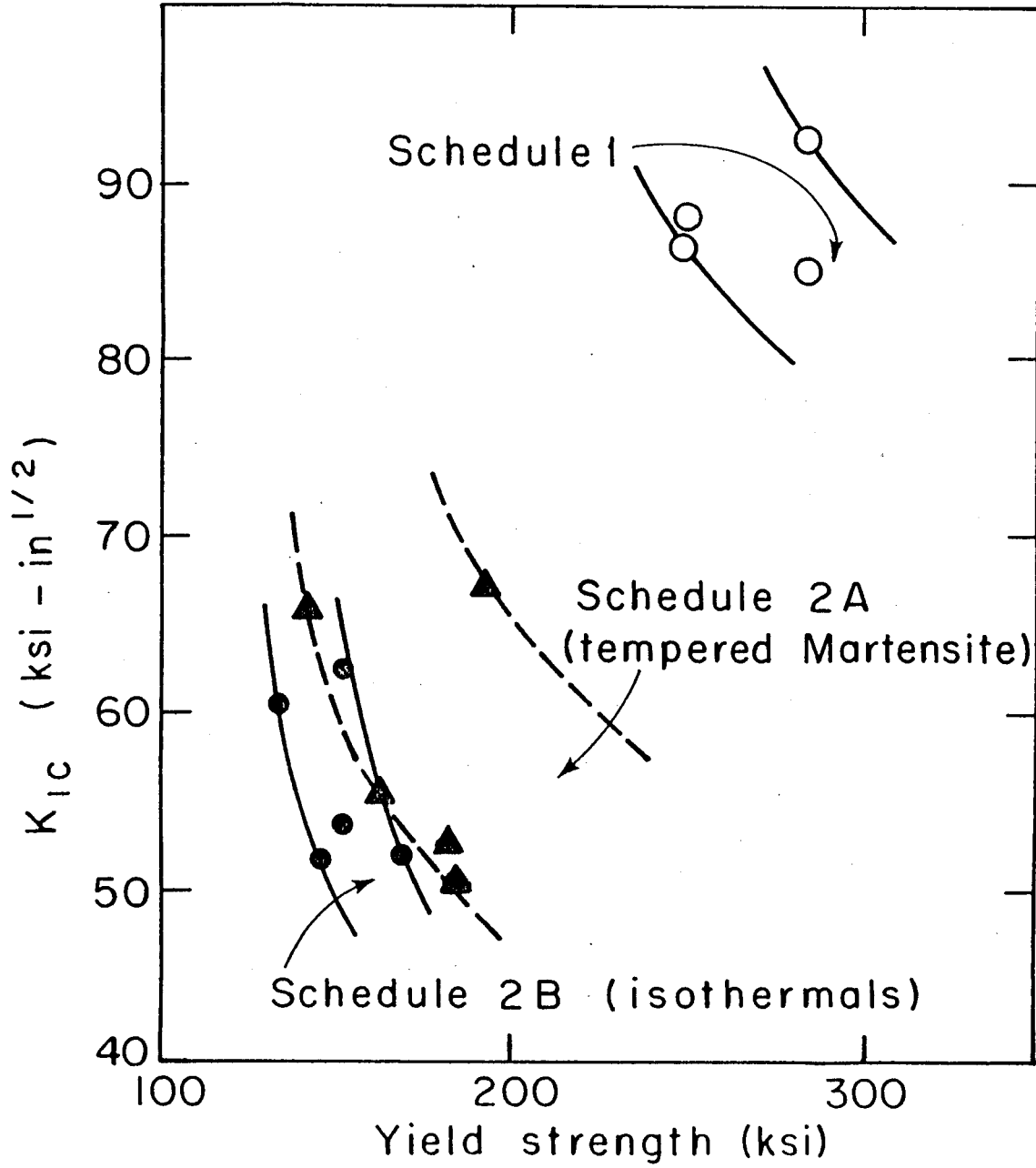
XBB 768-7577

Fig. 32.



XBL 768-3315

Fig. 33.



XBL 768-3338

Fig. 34.

ENTR MEM:B #MATRIX  
♦ ZAF MEM:B V=30 S=30 T=54.3  
ELEM LINE STD.  
FE K Q=99  
CR K  
V K  
MO K  
W L

+++++++  
87.646 %FE  
5.679 %CR  
1.025 %V  
2.358 %MO  
2.289 %W  
♦

ENTR MEM:A #CARBIDE  
♦ ZAF MEM:A V=30 S=30 T=54.3  
ELEM LINE STD.  
FE K Q=90  
CR K  
V K  
MO K  
W L

+++++++  
41.978 %FE  
5.248 %CR  
2.477 %V  
18.695 %MO  
21.599 %W  
♦

XBL 768-8997

Fig. 35.

ENTR MEM:A #303 CARBIDE B  
♦ ZAF MEM:A V=30 S=  
♦ ZAF MEM:A V=20 S=30 T=41  
ELEM LINE STD.  
V K Q=98  
CR K  
FE K  
MO L  
W M  
SI K

\*\*\*\*\*  
2.704 %V  
2.451 %CR  
23.138 %FE  
28.774 %MO  
39.735 %W  
1.135 %SI  
♦

ENTR MEM:A #302 MATRIX  
♦ ZAF MEM:A V=20 S=30 T=33  
ELEM LINE STD.  
V K Q=100  
CR K  
MN K  
FE K  
SI K  
MO L  
W M

\*\*\*\*\*  
1.008 %V  
4.131 %CR  
.139 %MN  
39.386 %FE  
1.711 %SI  
2.454 %MO  
.667 %W  
♦

ENTR MEM:B #303 MATRIX  
♦ ZAF MEM:B V=20 S=30 T=41  
ELEM LINE STD.  
V K Q=98  
CR K  
FE K  
MO L  
W M  
SI K

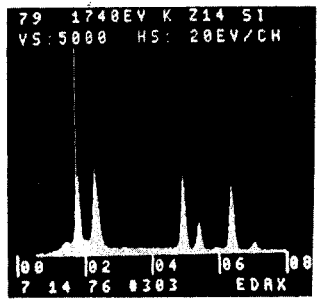
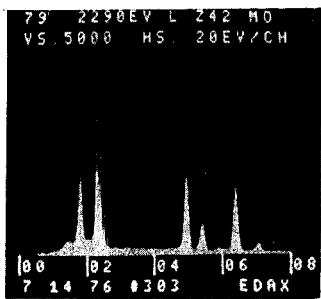
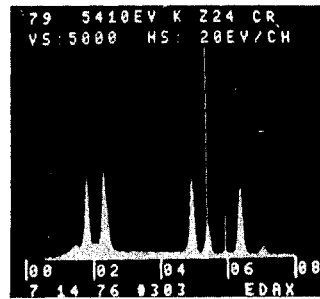
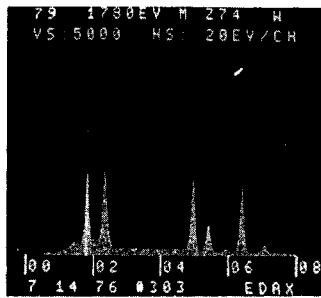
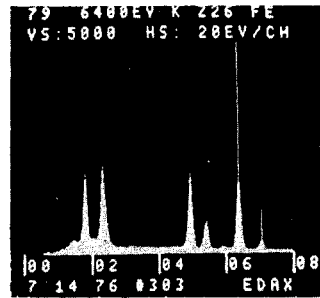
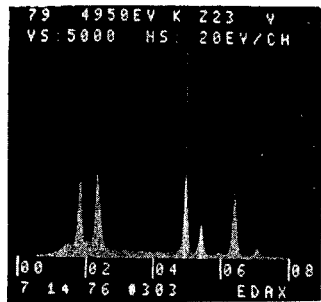
\*\*\*\*\*  
.600 %V  
4.363 %CR  
37.004 %FE  
2.420 %MO  
3.522 %W  
.089 %SI  
♦

ENTR MEM:A #302 CARBIDE  
♦ ZAF MEM:A V=20 S=30 T=33  
ELEM LINE STD.  
V K Q=98  
CR K  
MN K  
FE K  
SI K  
MO L  
W M

\*\*\*\*\*  
1.430 %V  
3.958 %CR  
26.040 %MN  
7.494 %FE  
2.066 %SI  
32.691 %MO  
2.318 %W  
♦

XBL 768-8998

Fig. 36.



XBB 768-7576

Fig. 37.



XBB 768-7578

Fig. 38.

ENTR MEM:A #302 CARBIDE  
♦ ZAF MEM:A V=20 S=30 T=33  
ELEM LINE STD.  
V K Q=93  
CR K  
MN K  
FE K  
SI K  
MO L  
W M

+++++++  
1.524 W  
3.256 CR  
21.155 MN  
12.300 FE  
4.566 SI  
48.585 MO  
4.010 W  
♦

ENTR MEM:A #302CARBIDE D2 C  
♦ ZAF MEM:A V=20 ??  
♦ ZAF MEM:A V=20 S=30 T=33  
ELEM LINE STD.  
V K Q=93  
CR K  
MN K  
FE K  
SI K  
MO L  
W M

+++++++  
1.167 W  
4.147 CR  
15.747 MN  
24.599 FE  
4.793 SI  
43.370 MO  
4.174 W  
♦

ENTR MEM:B #302 CARBIDE  
♦ ZAF MEM:B V=2030  
♦ ZAF MEM:B V=20 S=30 T=33  
ELEM LINE STD.  
V K Q=93  
CR K  
MN K  
FE K  
SI K  
MO L  
W M

+++++++  
15.599 W  
2.376 CR  
13.590 MN  
24.430 FE  
1.735 SI  
33.134 MO  
1.031 W  
♦

XBL 768-8999

Fig. 39.